PLOS PATHOGENS

RESEARCH ARTICLE

RNA structures within Venezuelan equine encephalitis virus E1 alter macrophage replication fitness and contribute to viral emergence

Sarah E. Hickson, Jennifer L. Hyde*

Department of Microbiology, University of Washington School of Medicine, Seattle, Washington, United States of America

* jlhyde4@uw.edu

OPEN ACCESS

Citation: Hickson SE, Hyde JL (2024) RNA structures within Venezuelan equine encephalitis virus E1 alter macrophage replication fitness and contribute to viral emergence. PLoS Pathog 20(9): e1012179. https://doi.org/10.1371/journal.ppat.1012179

Editor: Thomas E. Morrison, University of Colorado Denver, UNITED STATES OF AMERICA

Received: April 5, 2024

Accepted: September 3, 2024

Published: September 27, 2024

Data Availability Statement: All relevant data are within the manuscript and its Supporting Information files.

Funding: NIH grant R01 AI155416 (JLH) and UW Royalty Research Fund A172539 (JLH) supported this work. This work is supported in part by the University of Washington's Proteomics Resource (UWPR95794), the Genomics & Bioinformatics Shared Resource, RRID:SCR_022606, of the Fred Hutch/University of Washington/Seattle Children's Cancer Consortium (P30 CA015704) and the Office

Abstract

Venezuelan equine encephalitis virus (VEEV) is a mosquito-borne +ssRNA virus belonging to the *Togaviridae*. VEEV is found throughout Central and South America and is responsible for periodic epidemic/epizootic outbreaks of febrile and encephalitic disease in equines and humans. Endemic/enzootic VEEV is transmitted between Culex mosquitoes and sylvatic rodents, whereas epidemic/epizootic VEEV is transmitted between mosquitoes and equids, which serve as amplification hosts during outbreaks. Epizootic VEEV emergence has been shown to arise from mutation of enzootic VEEV strains. Specifically, epizootic VEEV has been shown to acquire amino acid mutations in the E2 viral glycoprotein that facilitate viral entry and equine amplification. However, the abundance of synonymous mutations which accumulate across the epizootic VEEV genome suggests that other viral determinants such as RNA secondary structure may also play a role in VEEV emergence. In this study we identify novel RNA structures in the E1 gene which specifically alter replication fitness of epizootic VEEV in macrophages but not other cell types. We show that SNPs are conserved within epizootic lineages and that RNA structures are conserved across different lineages. We also identified several novel RNA-binding proteins that are necessary for altered macrophage replication. These results suggest that emergence of VEEV in nature requires multiple mutations across the viral genome, some of which alter cell-type specific replication fitness in an RNA structure-dependent manner.

Author summary

Understanding how viral pathogens emerge is critical for ongoing surveillance and outbreak preparedness. However, our understanding of the molecular mechanisms that drive viral emergence are still not completely understood. Emergence of the mosquito-borne virus Venezuelan equine encephalitis virus (VEEV) is known to require mutations in the viral attachment protein (E2), which drive viremia and transmission. We have observed that emergent strains (epizootic VEEV) also accumulate many silent mutations,

of the Director, National Institutes Of Health of the National Institutes of Health (S10OD026741). The funders had no role in study design, data collection and analysis, decision to publish, or preparation of the manuscript.

Competing interests: The authors have declared that no competing interests exist

suggesting that other determinants independent of protein sequence also contributes to emergence. In this study we identify novel RNA secondary structures associated with epizootic VEEV that alters viral replication in a cell-type dependent manner. We show that these RNA structures are conserved across epizootic viruses and identify host proteins that specifically bind these RNAs. These findings imply that viral emergence requires multiple mutations, a number of which likely alter viral RNA structure in a manner that benefits viral replication and transmission.

Introduction

Alphaviruses are a group of enveloped positive-sense RNA (+ssRNA) viruses belonging to the *Togaviridae* family. These viruses are transmitted by arthropod vectors and are etiological agents of several significant human and veterinary diseases. Alphaviruses are globally distributed and can be broadly classified in two groups based on their associated pathologies, chiefly arthritogenic or encephalitic. Venezuelan equine encephalitis virus (VEEV) causes periodic outbreaks of febrile and encephalitic disease in equids and humans throughout Central and South America [1]. Endemic/enzootic VEEV is predominantly transmitted between *Culex (Melanoconion)* spp. mosquitoes and sylvatic rodents such as cotton rats and spiny rats which are believed to be the major reservoir host for these endemic/enzootic viruses (subtypes ID and IE) [2]. Emergence of epidemic/epizootic VEEV (subtypes IAB and IC) occurs de novo via mutation of enzootic subtypes [3]. In contrast to endemic/enzootic VEEV, epidemic/epizootic subtypes are primarily transmitted between several mammalophilic mosquitoes and equines which are the major amplification hosts during these outbreaks [4,5]. Spillover infections into humans also occur during epidemic/epizootic episodes and can be associated with severe encephalitic disease and death, as well as long-term debilitating sequelae [6]. Repeated emergence of epidemic/epizootic VEEV has previously been shown to involve mutation of the viral attachment protein (E2) of ID endemic/enzootic subtypes which give rise to epidemic/epizootic VEEV subtypes IAB and IC [7–9]. E2 mutations were found to facilitate increased replication levels in horses, heightened virulence, and adaptation to epizootic mosquito vectors [4,10]. While these mutations alone have been demonstrated to be sufficient for imparting epizootic phenotypes in a laboratory setting, epidemic/epizootic subtypes contain numerous additional mutations across the viral genome which studies suggest may contribute to epidemic/epizootic emergence [11,12].

The VEEV genome is approximately 11.5kb in length and contains a 5'methylguanosine (m7G) cap and a 3' polyA tail [13]. The genome consists of two open reading frames, ORF1 which encodes four non-structural proteins (nsp1-4) and ORF2 which encodes a subgenomic RNA from which the viral structural proteins are translated. We have previously shown that RNA structures present in the 5'UTR of the VEEV and Sindbis virus (SINV) confer resistance to the interferon stimulated gene (ISG) IFIT1, by preventing IFIT1 recognition of viral m7G capped RNA [14]. Similarly, we have observed that changes in VEEV 3'UTR structure alters IFIT2-mediated restriction of viral replication in a subtype-dependent manner [15]. Notably, most SNPs acquired by epidemic/epizootic strains following VEEV emergence are synonymous, suggesting that in addition to protein coding mutations in E2, changes in viral RNA structure may contribute to emergence of epidemic/epizootic VEEV. In this study we identify novel RNA structures in E1 that alter replication in macrophages which are early targets of VEEV infection in vivo. Conservation of SNPs and RNA secondary structures in this region

suggest that these structures may contribute to emergence of epidemic/epizootic VEEV. These findings have significance for our understanding of VEEV evolution and emergence.

Results

To first identify putative RNA structures that differ between endemic/enzootic and epidemic/epizootic strains we used phylogenetic analysis to identify closely related pairs of enzootic and epizootic strains for subsequent RNA structure analysis (**S1 Fig**). We compared 143 isolates and identified three enzootic (subtype ID) strains (R16905, 307537, and 204381) which exhibited 99.4%, 96.5%, and 96.2% sequence identity to the epizootic (subtype IAB) vaccine strain TC83. For downstream RNA structure analysis, we chose to compare TC83 and 307537. TC83 is a BSL2 attenuated vaccine strain developed by serial passage of strain Trinidad donkey (TRD) which was originally isolated from a sick donkey during an epizootic outbreak in Trinidad [13,16]. TC83 shows 99.9% sequence identity with TRD but contains attenuating mutations in the 5'UTR and the viral attachment protein E2 [13,16]. 307537 is a geographically distinct strain first isolated from mosquitoes and shares 96.5% sequence identity with TC83. To determine the predicted secondary structure of each viral genome, we used RNAfold [17,18, 19, 20] to perform a sliding window analysis of each strain and generate an RNA structure score (RSS) for each window (**Fig 1B**). The RSS is generated by dividing the frequency of the minimum free energy structure (MFE) by the ensemble diversity (ED), and thus captures some qualitative data of RNA secondary structures formed by that sequence. In this instance, a higher RSS suggests the presence of RNA structures which are more thermodynamically stable and have a higher probability of forming. By reducing the complexity of RNA secondary structure to a single numerical value, we can compare large groups of sequences (e.g. phylogenetic analysis) and identify RNA 'signatures' which may be unique or conserved within these groups. Our analysis revealed several regions with highly stable putative RNA structures (z-score >2), including nsp1, nsp2, nsp4, capsid, and E1 (**Fig 1B**, **S2 Fig**). Previously defined functionally relevant RNA structures were also identified using this analysis, notably the nsp1 packaging signal [21], and the ribosomal frameshift (RFS) motif in 6K/E1 which is required for production of TF protein [22,23]. In addition, we identified several regions in which the predicted RNA structure differed between TC83 and 307537, including within E1 (**Fig 1C**). As we observed a high proportion of synonymous mutations in this gene (97.6%; **Fig 1A**) and have previously shown that RNA structures proximal to this gene (3'UTR) alter replication properties of VEEV [15], we sought to define the role of E1 RNA structures in viral replication and their potential contribution to emergence of epizootic VEEV.

To determine whether changes in predicted E1 RNA structures alter VEEV replication properties, we generated a chimeric TC83 virus encoding all synonymous changes from E1 of strain 307537 (TC83/E1$_{IDsyn}$) (**Fig 2A**). To disentangle confounding effects of amino acid changes on replication phenotypes, this chimera excluded the single protein coding mutation found within this region (nucleotide (nt) 10,481, **Fig 1C**). Notably, inclusion of this mutation in our structure analysis did not significantly alter the RSS in this region, and thus was predicted to have minimal effect on E1 RNA structure (**Fig 1C**). We then compared replication kinetics of TC83 and TC83/E1$_{IDsyn}$ in several cell types including the macrophage cell line Raw264.7, primary bone marrow-derived macrophages (BMDM), primary bone marrow derived dendritic cells (BMDC), and mouse embryonic fibroblasts (MEF) (**Fig 2B-2E**). Here, cells were infected with WT or mutant viruses at an MOI of 0.1 and production of infectious virus measured over time by focus forming assay (FFA). Myeloid cells including macrophages are early targets of encephalitic alphavirus infection in vivo and have been shown to be a source of type I IFN production early during infection [24,25]. Thus, replication fitness in

A

Gene	SNPs	Synonymous		Non-synonymous	
		#	%	#	%
5'UTR	2	2	100	-	-
nsp1	35	33	94.3	2	5.7
nsp2	86	76	88.4	10	11.6
nsp3	61	47	77	14	23
nsp4	73	71	97.3	2	2.7
SGP	0	-	-	-	-
capsid	32	27	84.4	5	15.6
E3	3	3	100	-	-
E2	57	41	71.9	16	28.1
6K	7	5	71.4	2	28.6
E1	41	40	97.6	1	2.4
3'UTR	6*	6*	100	-	-
Total	**403**	**351**	**87.1**	**52**	**12.9**

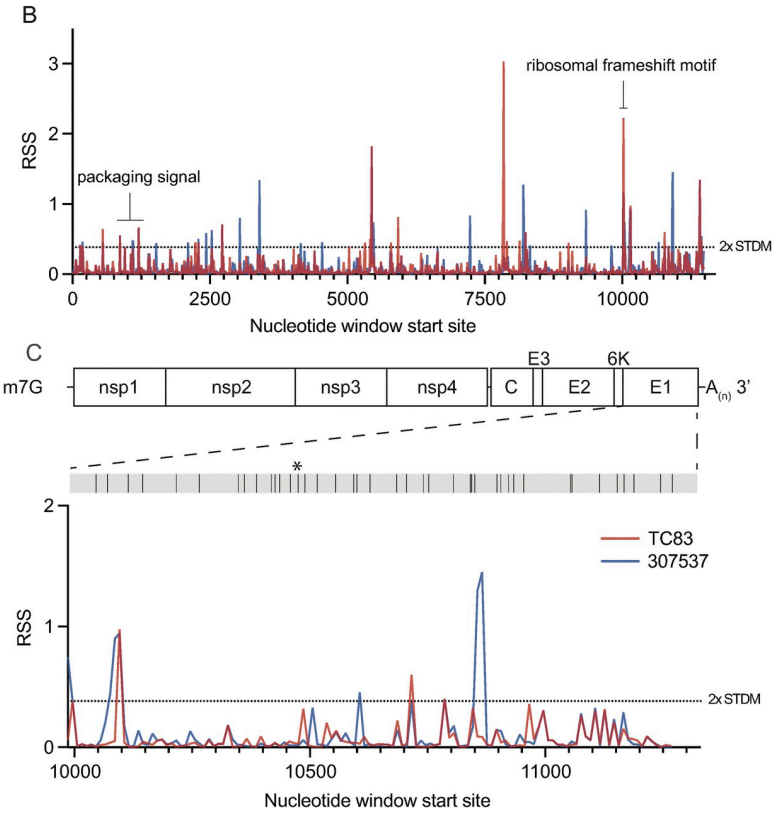

Fig 1. Predicted RNA secondary structure of E1 differs between epizootic and enzootic VEEV. (A) Summary of all SNPs identified between TC83 and 307537. (B) RNA structure analysis of subtype IAB and ID VEEV. RNA structure prediction of VEEV strain TC83 (IAB; accession L01443) and strain 307537 (ID; accession KC344519) was performed using RNAfold [17] (window size = 50nt, step size = 10 nt). The RNA structure score (RSS; frequency of MFE/ensemble diversity) is plotted against the nt window start site. Higher RSS indicates greater thermodynamic stability of predicted structures. The 2-fold standard deviation is indicated by a dotted line. (C) RSS analysis of gene E1 from strains TC83 and 307537. Location of all SNPs across E1, including a single coding change (*), are depicted in the grey bar above.

https://doi.org/10.1371/journal.ppat.1012179.g001

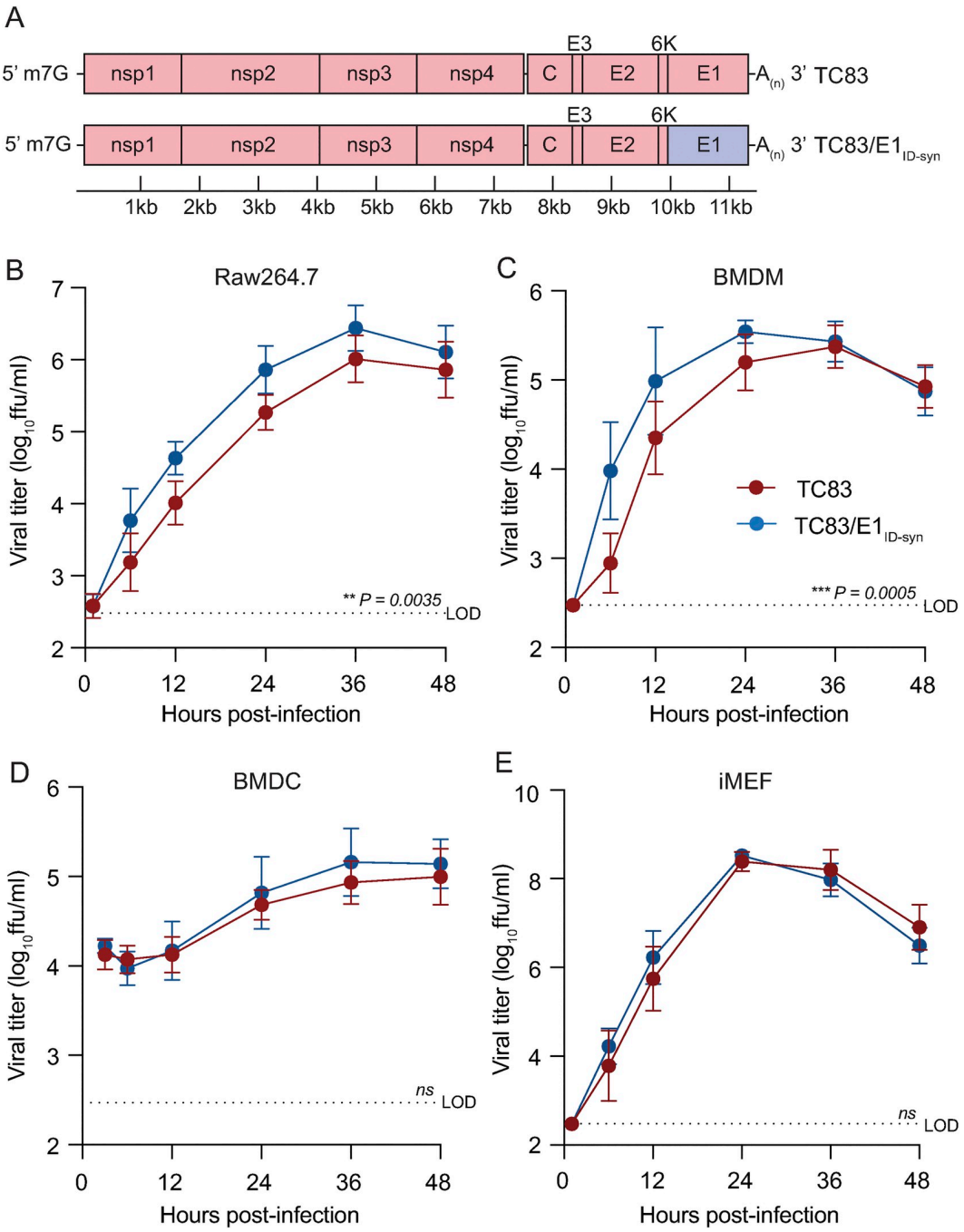

Fig 2. Changes in E1 RNA sequence alters viral replication fitness in macrophages, but not other cell types. (A). Schematic representation of the TC83 and TC83 E1 RNA mutant (TC83/E1$_{ID\text{-}syn}$) genomes. Synonymous SNPs from E1 of enzootic VEEV (strain 307537) were introduced into the vaccine epizootic VEEV (strain TC83) to generate an RNA mutant (TC83/E1$_{ID\text{-}syn}$). The single coding change present in E1 (Fig 1C, asterisk) was omitted from the mutant. Red denotes sequences from the parent epizootic strain (TC83), and blue denotes sequences from the enzootic strain (307537). **(B-E).** Replication kinetics of VEEV TC83 and TC83/E1$_{ID\text{-}syn}$ in **(B)** Raw264.7, **(C)** primary bone marrow-derived macrophages (BMDMs), **(D)** primary bone marrow-derived dendritic cells (BMDCs), and **(E)** immortalized mouse embryonic fibroblasts (iMEF). Cells were infected with indicated viruses at a MOI of 0.1 (Raw264.5, BMDMs, iMEF) or MOI 0.01 (BMDCs). Cell culture supernatant was serially harvested at 1, 6, 12, 24, 36, and 48 hpi and infectious virus was titered using focus forming assay (FFA). Each experiment was performed in triplicate three to four times independently and the mean and SD are graphed. Statistical analysis was performed by calculating the area under the curve (AUC) for each replicate, and the AUC values from WT and mutant viruses were analyzed by unpaired t-test.

https://doi.org/10.1371/journal.ppat.1012179.g002

macrophages would be predicted to have significant impacts on outcomes of VEEV infection *in vivo*. In both Raw264.7 and primary BMDM we observed an increase in TC83/$E1_{IDsyn}$ relative to TC83 (at 12hpi, 8-fold in Raw264.7, $P = 0.0035$; 10-fold in BMDM, $P = 0.0005$) (**Fig 2B and 2C**). Remarkably, we observed no significant difference in replication of TC83 and TC83/$E1_{IDsyn}$ in either BMDC or MEF (**Fig 2D and 2E**), indicating that RNA sequences from E1 of enzootic VEEV specifically increases replication fitness in macrophages but not in other cell types.

Type-I IFN is important in restricting replication and pathogenesis of alphaviruses [26–28], and we have previously shown that VEEV RNA structure facilitates evasion of IFN-stimulated genes (ISGs) [14,15]. Thus, we hypothesized that putative E1 RNA structures from TC83/$E1_{IDsyn}$ could enhance replication in macrophages by facilitating evasion of host antiviral immunity. Specifically, we predicted that mutant E1 RNAs may evade sensing of VEEV RNA by RLRs RIG-I and MDA-5 which are known to play a role in alphavirus RNA sensing, particularly of 3' RNAs [29,30]. To test this hypothesis, we used CRISPR to generate *Ddx58* and *Ifih1* knock out (KO) Raw264.7 macrophages and compared replication kinetics of TC83 and TC83/$E1_{ID\text{-}syn}$ in these cells (**Fig 3A-3C**; **S3 Fig**). Contrary to our expectations, TC83 replication was still impaired relative to TC83/$E1_{ID\text{-}syn}$ in both the absence and presence of RIG-I or MDA-5 expression (**Fig 3A-3C**). To confirm these data, we used transient siRNA knock down of *Ddx58* and *Ifih1*, as well as *Irf3* (**Fig 3D**; **S3 Fig**) and examined titers of TC83 and TC83/$E1_{ID\text{-}syn}$ compared to cells treated with a non-silencing control (NSC) siRNA. We predicted that if enhanced replication of TC83/$E1_{IDsyn}$ was due to evasion of RLR-dependent sensing and antiviral restriction then knock down of RLR expression or expression of downstream signaling molecules (IRF3) would result in an increase in replication of TC83 but no change in the replication of TC83/$E1_{ID\text{-}syn}$. However, consistent with CRISPR data, we observed no increase in replication of TC83 in the absence of either RLR expression or IRF3. Furthermore, knockdown of *Irf3* did not lead to an increase in TC83 replication relative to TC83/$E1_{ID\text{-}syn}$, suggesting that preferential sensing and/or inhibition of TC83 RNA cannot explain the observed replication differences in macrophages.

While these data did not support a role of RLR-mediated RNA sensing in differential replication of TC83 and TC83/$E1_{ID\text{-}syn}$, we could not rule out a role for other RNA sensing pathways or antiviral effectors which are independent of these pathways. As antiviral signaling pathways converge on expression of type-I IFNs which are critical for restriction of alphaviruses through expression of antiviral effectors, we examined whether differences in type-I IFN signaling and ISG expression accounted for enhanced replication of TC83/$E1_{ID\text{-}syn}$. To determine whether infection with TC83 or TC83/$E1_{ID\text{-}syn}$ led to differential activation of type-I IFN responses, Raw264.7 were treated with antibodies specific for the IFN-alpha receptor (IFNAR) or an IgG isotype control antibody prior to and during infection (**Fig 3E**). We expected that if diminished TC83 replication was due to impaired evasion of RNA sensing and IFN activation then IFNAR blockade would result in an increase in viral replication to levels similar to the mutant. However, while IFNAR blockade led to a significant inhibition of ISG expression as measured by qRT-PCR (**Fig 3F-3H**), neither infectious viral titers nor viral RNA production were affected when compared to treatment with an isotype control (**Fig 3E and 3I**). Collectively, this data suggests that differential replication of TC83 and TC83/$E1_{ID\text{-}syn}$ cannot be explained by altered evasion or induction of IFN or ISG expression by either virus.

To unveil what IFN-independent mechanisms might underlie the observed differences in TC83 and TC83/$E1_{ID\text{-}syn}$ replication (**Fig 2**), we used a proteomics approach to identify host proteins which interact differently with TC83 and TC83/$E1_{ID\text{-}syn}$ RNA. We hypothesized that changes in primary sequence and/or secondary structure could alter the viral RNA-protein interactome leading to changes in replication. Specifically, we predicted that antiviral RNA-

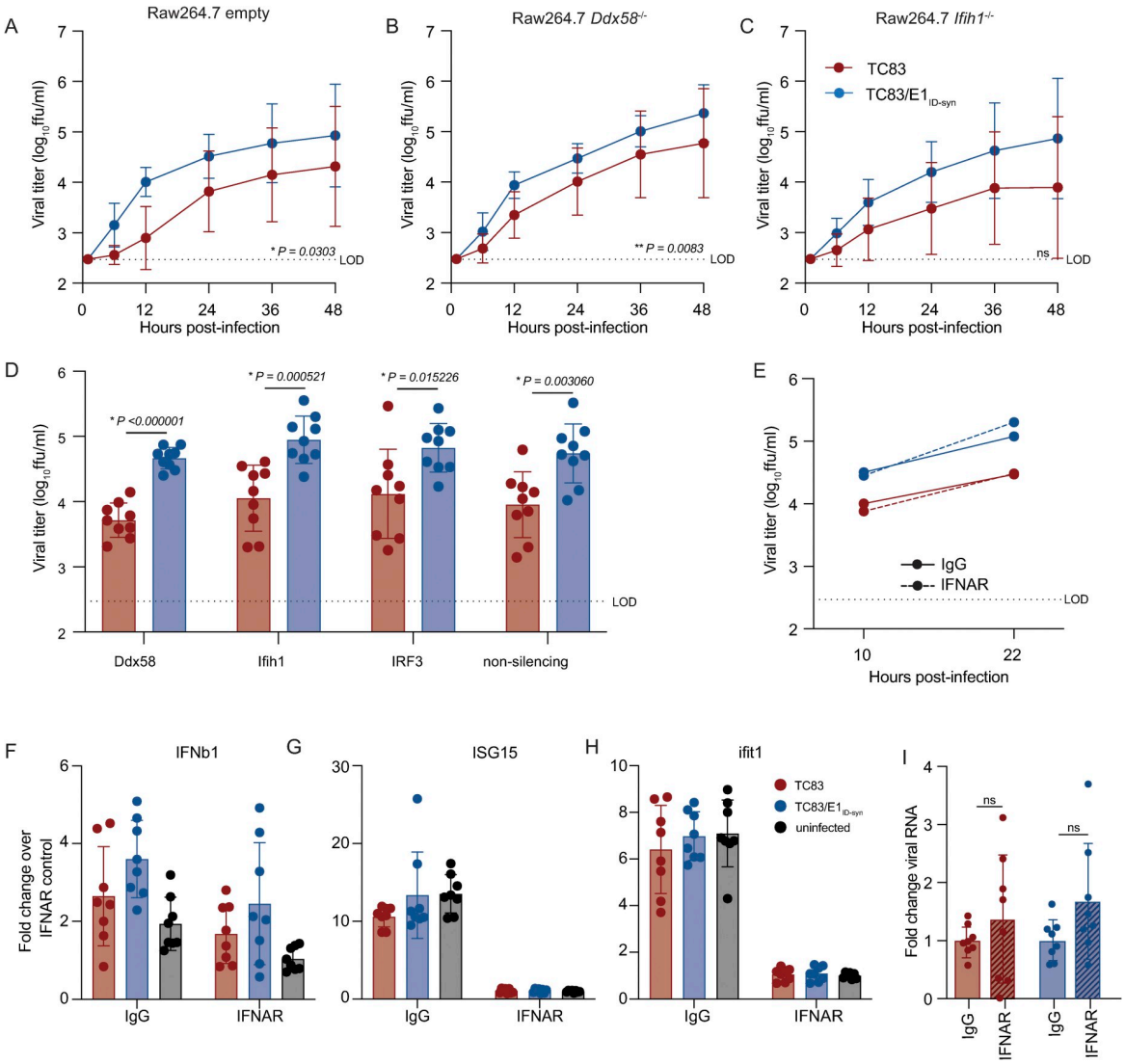

Fig 3. Differential macrophage replication of TC83 and TC83/E1$_{ID\text{-}syn}$ viruses is IFN- and RLR-independent. **(A-C)** Replication kinetics of VEEV TC83 and TC83/E1$_{ID\text{-}syn}$ in **(A)** empty vector, **(B)** *Ddx58*$^{-/-}$, and **(C)** *Ifih1*$^{-/-}$ CRISPR Raw264.7 cells. Cells were infected with indicated viruses at a MOI of 0.1. Cell culture supernatant was serially harvested at 1, 6, 12, 24, 36, and 48 hpi and infectious virus was titered using focus forming assay (FFA). Each experiment was performed in triplicate three times independently and the mean and SD are graphed. Statistical analysis was performed by calculating the area under the curve (AUC) for each replicate and experiment, and the AUC values for each virus analyzed by unpaired t-test. **(D)** Raw264.7 were treated with non-silecing control (NSC) siRNA or siRNA targeting *Mavs*, *Ddx58*, *Ifih1*, or *Irf3*. Cell culture supernatants were harvested at 24 hpi and infectious virus quantified by FFA. **(E)** Raw264.7 were pretreated for 1 hour with 10μg of IgG or IFNAR blocking antibody, then infected with TC83 or TC83/E1$_{ID\text{-}syn}$ at an MOI of 0.1 in the presence of antibody. Infectious virus from cell culture supernatants harvested at 10 and 22 hpi was titered by FFA. Each experiment was performed three times independently. **(F, G, H, I)** IFNAR blocking antibody assays were performed in WT Raw264.7 as described in E, and cell lysates collected at 22 hpi. IFNb1, ISG15, Ifit1 and VEEV viral RNA transcripts quantified by qRT-PCR. **(F, G, H)** Gene expression within samples was normalized to hprt, and fold change in gene expression relative to IFNAR samples was calculated. **(I)** Viral RNA fold change over IgG control was calculated and displayed per virus. Each experiment was performed three times independently in duplicate or triplicate, and statistical analysis was performed using unpaired t-test.

https://doi.org/10.1371/journal.ppat.1012179.g003

binding proteins (RBPs) would be enriched for TC83 RNA or that proviral RBPs would be enriched for TC83/E1$_{ID\text{-}syn}$ RNA. To define the RNA-protein interactome of TC83 or TC83/E1$_{ID\text{-}syn}$, Raw264.7 were infected at MOI 0.1 and viral RNA immunoprecipitated at 24 hpi using the J2 anti-dsRNA antibody [31]. RNA-bound protein targets were then purified and

identified using Liquid chromatography–mass spectrometry (LC-MS). A total of 166 proteins were identified (S1 Data). Differential enrichment of protein targets for each virus was calculated and targets prioritized as follows: (i) targets with spectral counts >10; (ii) targets showing >2-fold enrichment over the paired IgG control in at least one sample; (iii) targets showing >2-fold enrichment in TC83 vs TC83/E1$_{ID\text{-}syn}$ (or vice versa); (iv) targets with known RBP activity (based on RBPbase and GO terms). While MS data was generated from two independent experiments (Fig 4), we observed much lower spectral counts for targets in the second experiment as well as lower enrichment scores overall. Nonetheless, we identified several targets in both screens that were either differentially enriched for the WT or mutant virus (>1.5-fold; FBL, NOP58, CHTOP) or which were enriched equally for both (DHX9, ADAR, YBX1). Based on the more robust nature of the data set, downstream targets chosen for validation were based on data from experiment 1. Based on the criteria above we identified a total of 24 RBPs which showed differential binding to either the TC83 or TC83/E1$_{ID\text{-}syn}$ genomes (Fig 4A). In addition, we also identified several highly abundant targets (YBX1, HNRNPC, HNRNPM, and ADAR1) that were equally enriched for both viruses which have also been identified in previous studies as interacting with alphavirus RNA and would not be expected to be differentially enriched [32–34](Fig 4B). Remarkably, with the exception of UBTF and DHX38, all identified targets were found to be enriched for the mutant, suggesting that enhanced replication of TC83/E1$_{ID\text{-}syn}$ is not due to evasion of antiviral factors that restrict TC83, but recruitment of proviral RBPs to TC83/E1$_{ID\text{-}syn}$. Pathway analysis of these top hits showed enrichment for RBPs associated with snoRNAs and more broadly RNA metabolism (Fig 4C). To validate IP-MS findings and determine which RBPs were necessary for enhanced viral replication of TC83/E1$_{ID\text{-}syn}$ in macrophages, we used siRNA to inhibit expression of 11 of these targets in Raw264.7 and assess replication of WT and mutant viruses in these cells (Fig 4E-4H, S4 Fig). Here, Raw264.7 were transfected with NSC siRNA or a pool of 3 gene-specific siRNAs, infected with TC83 and TC83/E1$_{ID\text{-}syn}$ at MOI 0.1, and infectious virus quantified from supernatants by FFA. We observed that knock down of four of these targets (*Thrap3*, *Fbl*, *Ubap2l*, and *Dhx38*) led to reduced TC83/E1$_{ID\text{-}syn}$ replication to levels comparable to TC83, as compared to NSC-treated cells. Association of these RBPs with viral RNA was also validated using affinity purification (S12 Fig). To exclude the possibility that increased cell death following gene knock down could account for non-specific changes in viral replication in siRNA versus NSC treated cells we also measured cell viability in siRNA treated cells following infection at 24hpi (S4 Fig, **C**). Here, we observed no change, or only modest changes in cell viability which could not account for the decrease in TC83/E1$_{ID\text{-}syn}$ replication observed. To determine whether the cell type specificity of the TC83/E1$_{ID\text{-}syn}$ replication phenotype was due to cell-type dependent expression of RBPs, we additionally measured expression of TRAP3, DHX38, and FBL protein in Raw264.7 and MEF (S4 Fig **D and E**). Interestingly, we observed no difference in the expression of FBL and DHX38 between Raw264.7 and MEF, but contrary to expectations we observed a 4-fold increase in THRAP3 protein levels in MEF as compared to Raw264.7. Notably, expression of all three proteins was significantly reduced in MEF following viral infection but not in Raw264.7, suggesting that VEEV may downregulate expression of these RBPs in MEF but not macrophages, or that macrophages may be resistant to this down-regulation [35]. Collectively this data supports the hypothesis that these proteins are important for macrophage specific phenotype observed with TC83/E1$_{ID\text{-}syn.}$

We next sought to determine the possible mechanism by which these RBPs may alter viral replication in macrophages. RNA structures within the 3' end of viral genomes and host mRNAs, are known to be important for translation efficiency [36–38]. Interestingly, all four of the RBPs identified as being required for enhanced TC83/E1$_{ID\text{-}syn}$ replication in macrophages (FBL, THRAP3, UBAP2L, and DHX38) have been previously linked to regulation of mRNA

A

Target	Peptide counts TC83 a-IgG	TC83 a-dsRNA	TC83/E1$_{ID-syn}$ a-IgG	TC83/E1$_{ID-syn}$ a-dsRNA	Enrichment TC83/ TC83/E1$_{ID-syn}$	Enrichment TC83/E1$_{ID-syn}$ /TC83
Ehmt2	1	1	1	40	0.03	**40**
Syncrip	1	2	3	32	0.06	**16**
Bclaf1	1	2	1	25	0.08	**12.5**
Zc3h4	1	1	1	22	0.05	**22**
Hnrnpr	1	3	2	49	0.06	**16.33**
Krt76	2	1	1	16	0.06	**16**
Thrap3	2	3	2	48	0.06	**16**
Dsp	1	1	1	15	0.07	**15**
Jup	1	1	1	13	0.08	**13**
Fbl	17	21	11	100	0.21	**4.76**
Chtop	3	8	1	34	0.24	**4.25**
Tra2b	1	3	1	12	0.25	**4**
Gar1	1	4	1	15	0.27	**3.75**
Hnrnpu	18	26	23	74	0.35	**2.85**
Alyref	5	4	2	11	0.36	**2.75**
Nop56	20	23	16	61	0.38	**2.65**
Ubap2l	6	7	6	17	0.41	**2.43**
Hnrnpl	1	6	1	13	0.46	**2.17**
Acin1	1	10	1	20	0.5	**2**
Matr3	1	9	1	18	0.5	**2**
Nop58	11	16	8	32	0.5	**2**
Rpl31	4	6	5	10	0.5	**2**
Ubtf	15	41	9	13	**3.15**	0.32
Dhx38	6	12	1	5	**2.4**	0.42

B

Target	Peptide counts TC83 a-IgG	TC83 a-dsRNA	TC83/E1$_{ID-syn}$ a-IgG	TC83/E1$_{ID-syn}$ a-dsRNA	Enrichment TC83/ TC83/E1$_{ID-syn}$	Enrichment TC83/E1$_{ID-syn}$ /TC83
Adar	1	80	2	77	1.04	0.96
Ybx1	4	27	6	36	0.75	1.33
Hnrnpc	1	30	1	27	1.11	0.9
Hnrnpm	38	87	39	106	0.82	1.22
Dhx9	5	59	3	52	1.13	0.88

C

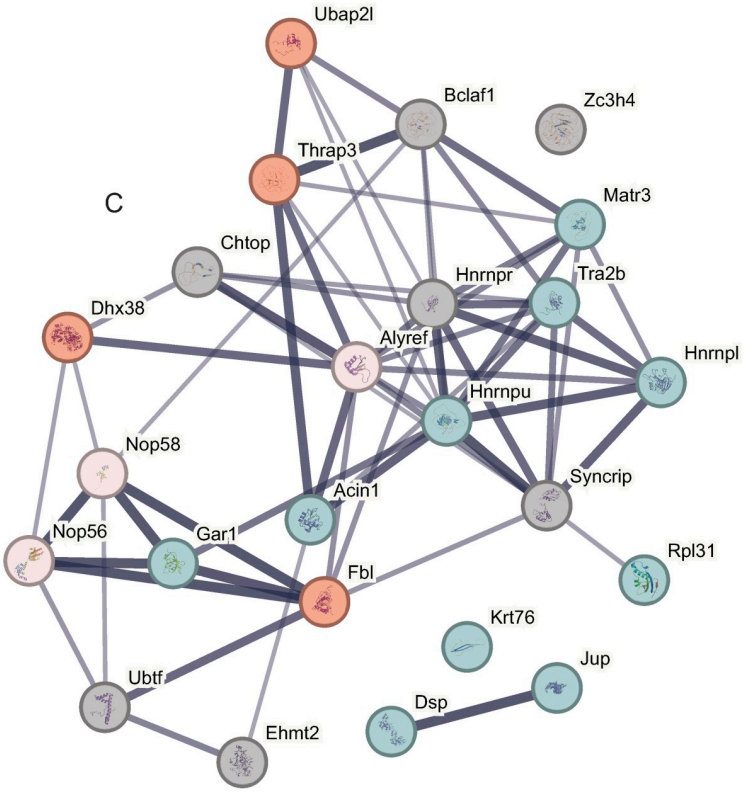

D

Biological process	GO #	Observed gene count	False discovery rate
RNA processing	GO:0006396	13	7.09E-08
Gene expression	GO:0010467	17	1.97E-07
RNA metabolic process	GO:0016070	15	1.97E-07
mRNA processing	GO:0006397	10	3.19E-07
mRNA metabolic process	GO:0016071	11	3.19E-07
Nucleic acid metabolic process	GO:0090304	16	8.08E-07
RNA splicing	GO:0008380	9	8.99E-07
RNA localization	GO:0006403	7	4.55E-06
Cellular nitrogen compound metabolic process	GO:0034641	17	4.22E-05
Regulation of mRNA metabolic process	GO:1903311	7	0.00012
Negative regulation of mRNA metabolic process	GO:1903312	5	0.00017
Regulation of mRNA splicing, via spliceosome	GO:0048024	5	0.00048

E

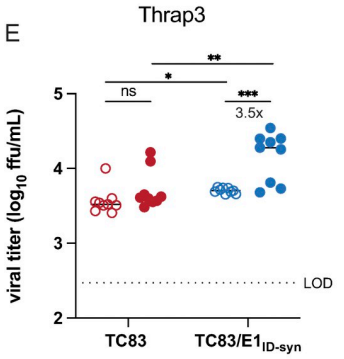

F

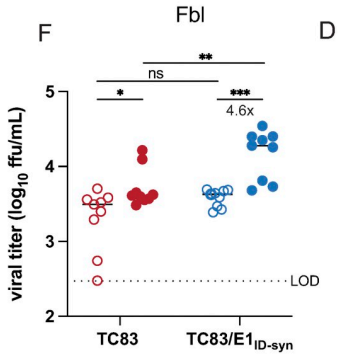

G

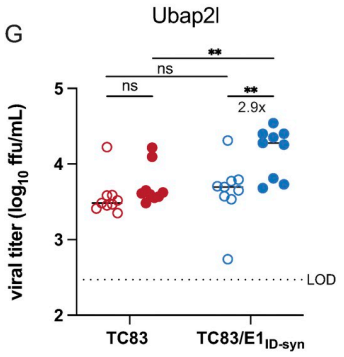

H

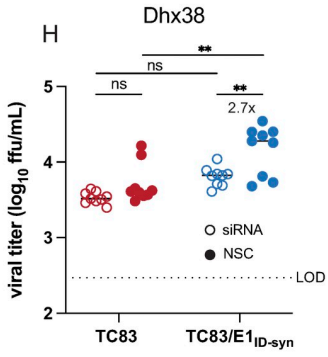

Fig 4. Increased macrophage replication fitness of TC83/E1$_{IDsyn}$ is dependent on expression of RNA binding proteins Fbl, Thrap3, Ubap2l, and Dhx38. (A) Top hits from dsRNA immunoprecipitation-mass spectrometry (IP-MS) of TC83 and TC83/E1$_{IDsyn}$ in Raw264.7. Raw264.7 cells were infected with TC83 or TC83/E1$_{IDsyn}$ at an MOI of 0.1, and viral dsRNA isolated from lysates at 24 hpi using J2 dsRNA antibody [31] or IgG isotype control. RNA-bound proteins were identified by MS, and fold-enrichment of spectral counts relative to IgG controls was calculated. Prioritized hits were chosen based on fold enrichment scores, total spectral counts, and whether targets are known RNA binding proteins (RBPbase hits). **(B)** Hits equally enriched in TC83 and TC83/E1$_{IDsyn}$. **(C)** STRING network analysis of top proteomics hits. Candidates meeting the cutoff criteria (A) were subjected to Protein-Protein Interaction Networks Functional Enrichment Analysis. Candidate proteins identified in the screen are highlighted in red and interacting proteins in blue. **(D)** Enriched biological process GO terms that with a p-value >0.001, along with the observed gene count present in the STRING network **(E-H)** Raw264.7 were transfected with control (NSC) or pooled (3 siRNA) gene specific siRNAs targeting **(E)** Thrap3, **(F)** Fbl, **(G)** Ubap2l, or **(H)** Dhx38 for 24 hours. Cells were infected TC83 or TC83/E1$_{ID\text{-}syn}$ at an MOI of 0.1, cell culture supernatants collected at 24hpi, and infectious virus titered by FFA. All siRNAs were assayed simultaneously but for visual clarity, data for each gene is shown separately along with the shared control siRNA samples. Each experiment was performed in triplicate three times independently and the mean and SD are graphed. Statistical analysis was performed using unpaired t-test. ** >0.001, ***>0.0001. Fold change and p-values are indicated on each graph.

https://doi.org/10.1371/journal.ppat.1012179.g004

stability and translation [39–41]. Thus, we hypothesized that FBL, THRAP3, UBAP2L, and DHX38 increase TC83/E1$_{ID\text{-}syn}$ replication by increasing translation of viral RNA. To test this hypothesis we modified a previously described VEEV luciferase translation reporter to include the E1 sequence from either TC83 or TC83/E1$_{ID\text{-}syn}$ and compared translation of reporter RNAs in Raw264.7 (**Fig 5A**) [14,42]. Raw264.7 cells were nucleofected with *in vitro* transcribed capped reporter RNA and luciferase activity measured at the indicated timepoints. We observed a significant increase in translation of TC83/E1$_{ID\text{-}syn}$ reporter RNA compared to TC83 starting as early as 30 minutes post-nucleofection (~1.3-fold) and increasing over time (2-fold at 240 min) (**Fig 5B**). To confirm that the observed differences in translation were not an artifact of the translation reporter system, we generated a nsp3-tagged nano-luciferase (nLuc) VEEV replicon containing firefly luciferase under control of the subgenomic promoter and compared replication of TC83 and TC83/E1$_{ID\text{-}syn}$ replicons in Raw264.7.(**Fig 5C**). Similar to the translation reporter assays described above, Raw264.7 cells were nucleofected with in vitro transcribed and capped replicon RNA and nLuc expression measured using Nano-Glo Dual-luciferase reporter assay system (Promega). Consistent with our translation reporter assay data (**Fig 5B**), we observed a significant increase in nLuc activity of TC83/E1$_{ID\text{-}syn}$ replicon RNA as compared to TC83 at 3 (3.5-fold) and 6 (4.5-fold) hours post-nucleofection, further confirming a role for translation in the increased replication of TC83/E1$_{ID\text{-}syn}$.

To further evaluate whether RNA synthesis was also impacted by changes in E1 RNA, we used RT-qPCR to measure the ratio of gRNA to subgenomic (sg) RNA in Raw264.7 following infection (MOI 5) with TC83 or TC83/E1$_{ID\text{-}syn}$ virus. We reasoned that if changes in E1 RNA sequence or structure specifically affected gRNA but not sgRNA synthesis this would lead to differences in the ratio of sgRNA-to-gRNA between TC83 and TC83/E1$_{ID\text{-}syn}$. Consistent with translation and replicon data, we observed no significant difference in the sgRNA-to-gRNA ratio between TC83 and mutant virus (**Fig 5D**)., suggesting that changes in E1 sequence are not only impacting gRNA translation and RNA synthesis but that sgRNA production is also likely impacted.

To further evaluate whether the RBPs identified specifically alter translation of TC83 and TC83/E1$_{ID\text{-}syn}$ RNA, Raw264.7 cells were transfected with gene-specific siRNAs then nucleofected with TC83 or mutant reporter RNA 24 hours later, and translation assays performed on cellular lysates at the indicated time points (**Fig 5G-5H**). We chose to focus on THRAP3 and UBAP2L due to their proposed interactions (**Fig 4C**) and their shared role in translational control and stress granule assembly [43,44]. We observed significant translational repression of both TC83 and TC83/E1$_{ID\text{-}syn}$ following treatment of cells with Ubap2l siRNA which led to inconsistencies in translation reporter data, thus we chose to omit this data from our study. Notably, UBAP2L is a ribosome-associate RBP that has been implicated in modulating global regulators of translation [41], thus it is not surprising that we consistently observed poor or no translation of reporter RNA in Ubap2l siRNA-treated cells. Consistent with our initial

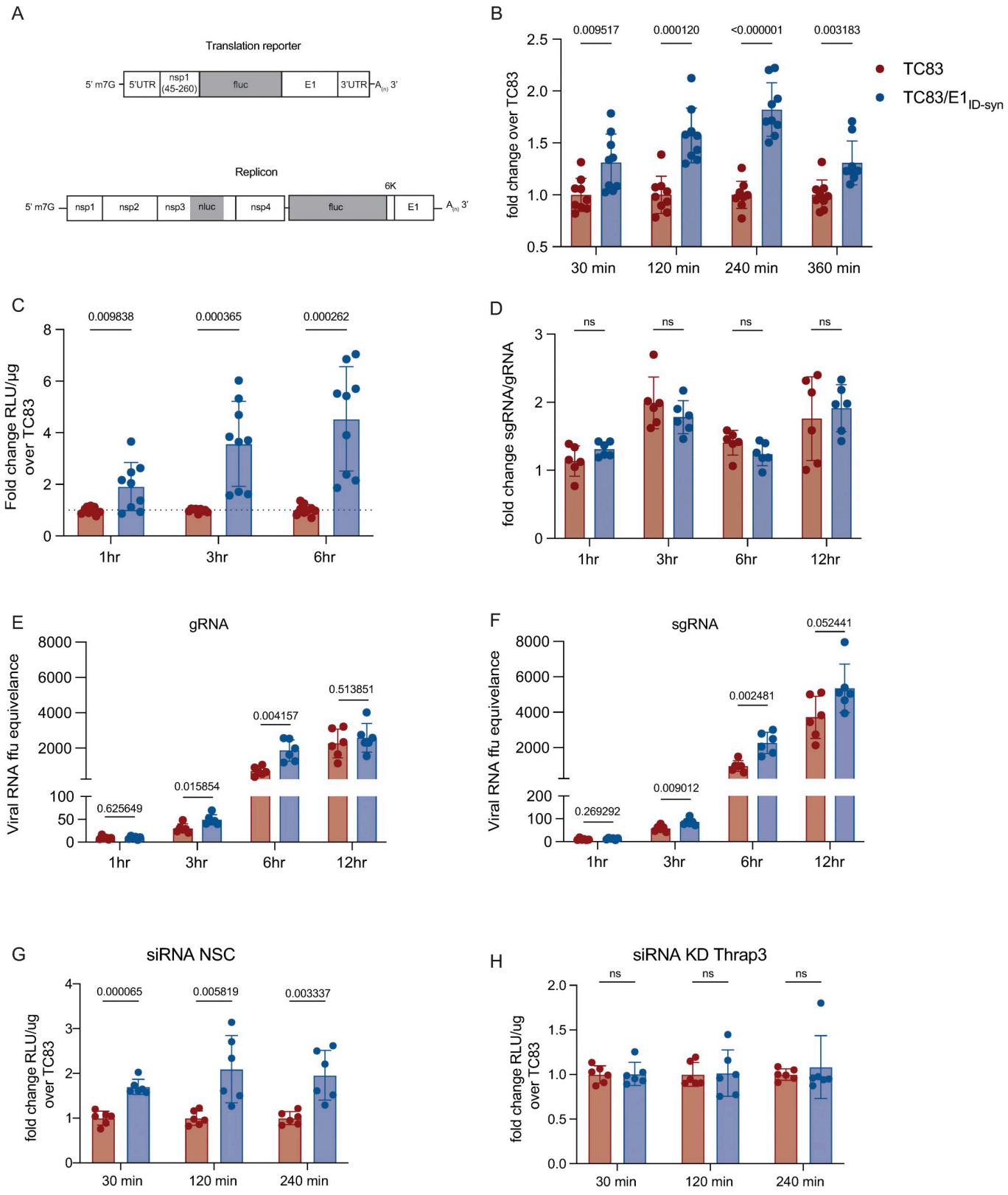

Fig 5. E1 RNA mutations alter translation and RNA transcription. (A) Schematic of translation reporter and replicon RNAs used. **(B)** 4μg of translation reporter RNA containing the E1 sequence from either TC83 or TC83/$E1_{ID\text{-}syn}$ were nucleofected into Raw264.7 macrophages. Cell lysates were collected at indicated times post nucleofection and luciferase activity measured. Data depicted as fold change over the TC83 samples for all time points. **(C)** 4μg nano/firefly

replicon reporter RNAs was nucleofected into Raw264.7 macrophages and cell lysates were harvested and dual-luciferase activity measured for indicated time-points. Nano-luciferase activity is displayed as fold change RLU/μg over TC83. **(D-F)** Raw264.7 were infected (MOI 1) with TC83 or TC83/E1$_{ID\text{-}syn}$ and lysates were harvested at 1, 3, 6 and 12hpi. RT-qPCR was performed using probes specific for genomic and sub-genomic RNA species. **(D)** the fold change between genomic and sub-genomic RNA per time point is displayed, **(E-F)** viral RNA ffu equivalence was calculated using a standard from RNA derived from a known concentration virus stock. **(G-H)** Raw264.7 were transfected with a non-silencing control (NSC) or Thrap3 siRNA and after 24hs cells were nucleofected with 4μg of translation reporter RNA constructs. Cell lysates were collected at indicated times post nucleofection and luciferase activity measured. The fold-change in RLU/μg is displayed for each time point. Each experiment was performed in duplicate or triplicate, three times independently and the mean and SD graphed. Statistical analysis was performed using an unpaired T-test.

https://doi.org/10.1371/journal.ppat.1012179.g005

translation reporter assay data (Fig 5B) we observed a significant increase (~2-fold) in translation of TC83/E1$_{ID\text{-}syn}$ RNA compared to TC83 in cells treated with NSC siRNA, but notably, KD of THRAP3 resulted in similar levels of luciferase activity for both reporters (Fig 5G and 5H). In fact, even partial KD of THRAP3 was sufficient to reduce translation of the TC83/E1$_{ID\text{-}syn}$ reporter RNA (S5 Fig). Collectively, our data shows that changes in E1 RNA sequence alter translation of viral RNA, and that enhanced translation of TC83/E1$_{ID\text{-}syn}$ is at least in part dependent on THRAP3.

Analysis of primary E1 sequences from TC83 and TC83/E1$_{ID\text{-}syn}$ failed to reveal obvious recognition motifs for any of the targets identified in our proteomics study. Thus, we generated additional E1 mutants to map regions within E1 necessary for differential macrophage replication and RBP recruitment (Fig 6A). Here, Raw264.7 cells were infected with parent or

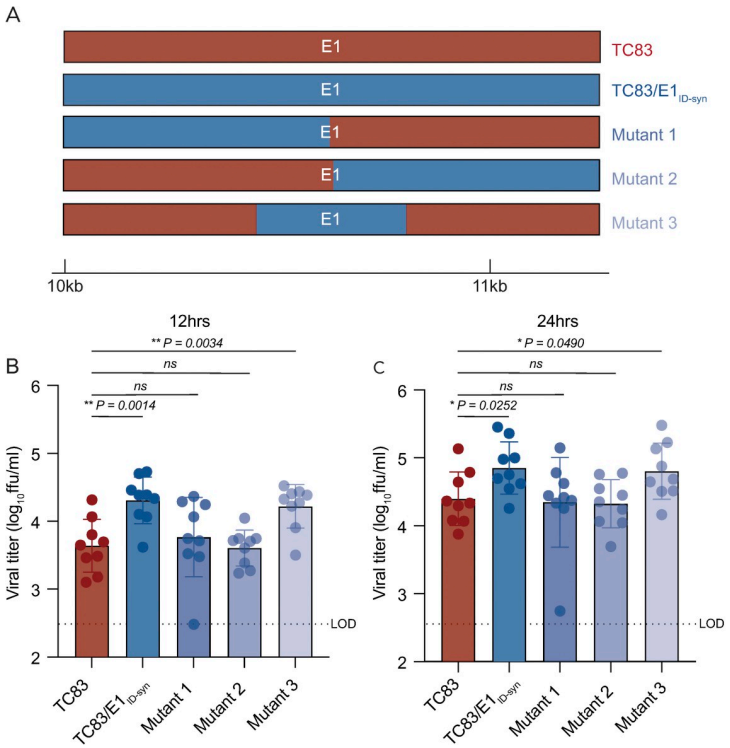

Fig 6. RNA sequences in the central domain of E1 enhance macrophage replication of TC83/E1$_{IDsyn}$. **(A)** Schematic representation of mutant viruses constructed. RNA chimeras containing 5' or 3' half or the central region of E1 synonymous mutations from TC83/E1$_{ID\text{-}syn}$ **(B, C)** Viral replication of chimeric viruses from Raw264.7 infected at MOI 0.1. Supernatants were harvested at 12 **(B)** or 24 **(C)** hpi and infectious virus titered by focus forming assay (FFA). Each experiment was performed in triplicate three times independently and the mean and SD graphed. Statistical analysis was performed using an unpaired T-test. * >0.05, ** >0.001.

https://doi.org/10.1371/journal.ppat.1012179.g006

mutant viruses at MOI of 0.1 and infectious titers at 12 and 24hpi were assessed by FFA (**Fig 6B and 6C**). We initially compared replication of two mutants in which the 5' or 3' half of E1 was exchanged between TC83 and TC83/$E1_{ID\text{-}syn}$ (mutant 1 and 2). Surprisingly, both mutant 1 and 2 replicated identically to the parent TC83 virus, suggesting that the element responsible for differential replication is located in the middle of E1 and was disrupted in these two mutants. To test this, we generated another mutant (mutant 3) which contained only SNPs from the central region of TC83/$E1_{ID\text{-}syn}$ E1 (nts 10,466–10,843) and compared replication of all viruses in Raw264.7 (**Fig 6B and 6C**). In contrast to mutant 1 and 2, mutant 3 replicated to similar levels as that of TC83/$E1_{ID\text{-}syn}$, confirming that the elements responsible for enhanced macrophage replication are located in the central region of E1.

We hypothesized that altered macrophage replication fitness was driven by changes in RNA structure, which alter binding of RBPs to viral RNA. Therefore, to determine whether SNPs in the central region of E1 altered the underlying structure of E1, we performed in-cell SHAPE-MaP [34,45] of cells infected with TC83 and TC83/$E1_{ID\text{-}syn}$. Here, Vero cells were infected with TC83 or TC83/$E1_{ID\text{-}syn}$ at an MOI of 0.1, treated with either DMSO (unreacted control) or the SHAPE chemical 1-methyl-7-nitroisatoic anhydride (1m7), and RNA lysates collected at 24hpi. SHAPE-MaP library preparation, sequencing, and analysis was performed as previously described [46], and SHAPE reactivity profiles generated for each viral genome (**Fig 7A**, **S7 Fig**). The SHAPE reactivity is indicative of the flexibility of each individual nucleotide, with low SHAPE reactivity correlating to paired nucleotides and high SHAPE reactivity correlating to unpaired nucleotides. Using these reactivity profiles as constraints for RNA folding, the secondary structure of TC83 and TC83/$E1_{ID\text{-}syn}$ E1 was determined using RNAfold (**Fig 7B and 7C**, **S6 Fig**). Within the central region of E1, we observed conservation of several secondary structural elements (in grey) between TC83 and TC83/$E1_{ID\text{-}syn}$. We also observed conservation of secondary structures in other regions of the viral genome, including the ribosomal frameshift motif in 6K/E1 (**S6 Fig**). Notably, our data was found to be consistent with previously published SHAPE-MaP analysis of VEEV strain ZPC738 [47] (**S6 Fig**) and we identified conserved secondary structures across all three viruses, lending further support to our findings. The central region of E1 responsible for the macrophage replication phenotype contains 11 SNPs (in blue). Three of these reside within the invariant RNA secondary structures identified (grey), and two SNPs (nts 10,481 and 10,633) were found to be unique to strain TC83 and another closely related IAB strain (AB66640; **S9 Fig**). Of the remaining six SNPs, three were found within regions that displayed the most variable RNA secondary structure (nts 10,522, 10,606, 10,810; **Fig 7A-7C**, boxed base pairs). To further define the SNPs responsible for enhanced TC83/$E1_{ID\text{-}syn}$ replication, we made an additional 5 TC83 mutants containing single point mutations at positions 10,495, 10,606, 10,747, 10,759, and 10,810 and compared replication of these viruses to TC83 and TC83/$E1_{ID\text{-}syn}$ in Raw264.7 (**S8 Fig**). Mutant 10,606 showed no increase in viral replication compared to TC83 at 12h or 24h. Of the remaining mutants tested, only 10,495 consistently showed an increase in replication at 12 and 24 hpi compared to TC83, whereas the other mutants (10,747, 10,759, and 10,810) replicated to levels similar to TC83 at 12hpi but showed increased replication similar to TC83/$E1_{ID\text{-}syn}$ at later times (24hpi). While the role of these three mutants in replication of TC83/$E1_{ID\text{-}syn}$ remains ambiguous, we can conclude from this data that at minimum SNPs that alter the 5' sequence of this E1 core region contribute to the enhanced replication of TC83/$E1_{ID\text{-}syn.}$ It is possible that complex interactions between RNA sequences is required for enhanced translation and replication, and that a combination of mutations is required to confer this phenotype. Since we hypothesized that changes in viral RNA structure contribute to emergence of epizootic VEEV in nature, we sought to determine whether SNPs were conserved across other epizootic or enzootic strains. We reasoned that RNA structures associated with epizootic emergence

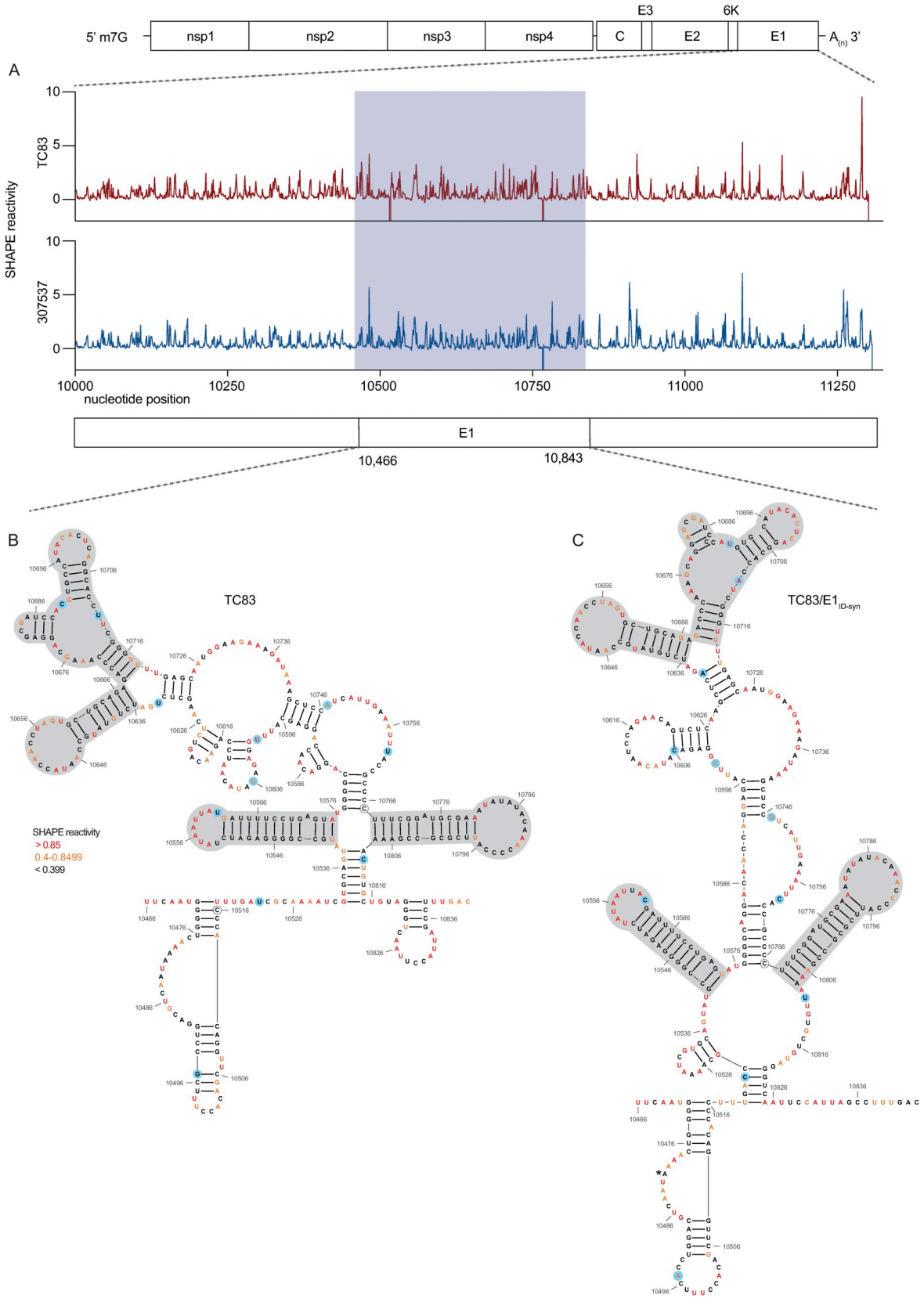
5' m7G
nsp1
nsp2
nsp3
nsp4
C
E3
E2
6K
E1
A(n) 3'
A
SHAPE reactivity
TC83
307537
nucleotide position
10000
10250
10500
10750
11000
11250
E1
10,466
10,843
B
TC83
SHAPE reactivity
> 0.85
0.4-0.8499
< 0.399
C
TC83/E1ID-syn

Fig 7. SHAPE-MaP analysis of TC83 and TC83/E1$_{IDsyn}$ infected cells. RNA from Vero cells infected with TC83 or TC83/E1$_{IDsyn}$ (MOI of 0.1) was analyzed by SHAPE-MaP. **(A)** Differential SHAPE reactivities of nucleotides in E1. The central region responsible for enhanced macrophage replication of TC83/E1$_{IDsyn}$ is highlighted in blue. Secondary structures and SHAPE reactivities of nucleotides in the central domain of **(B)** TC83 and **(C)** TC83/E1$_{IDsyn}$. Low reactive nucleotides (black) correspond to base-paired nucleotides and highly reactive nucleotides (orange, red) correspond to exposed bases. Structural elements conserved between both viruses are highlighted in grey, and SNPs are highlighted in blue.

https://doi.org/10.1371/journal.ppat.1012179.g007

would not be unique to TC83 but would also be present in other epizootic isolates. To this end, we compared sequences across 29 epizootic strains (subtype IAB and IC) and 40 enzootic strains (subtype ID) (S9 Fig). Indeed, with two exceptions, TC83 SNPs in the E1 central region were conserved across all IAB isolates. Phylogenetic analysis shows the presence of distinct lineages which largely correspond to distinct geographic distribution of these viruses [48–50]. Due to spatial evolution of these lineages, we speculated that epizootic-associated SNPs and RNA structures may also be lineage-specific, and not necessarily globally conserved across different lineages (compare epizootic sequences (red) within lineage K and lineage L). Indeed, when we compared epizootic IAB (TC83; lineage L) and epizootic IC sequences (lineage K), we observed SNPs distinct to epizootic viruses versus enzootic within the one lineage, but which were different between epizootic viruses across distinct lineages. While almost all TC83-associated SNPs in this region were conserved across other IAB isolates, we observed that in IC isolates only SNPs at position 10,495 and adjacent to 10,522 (yellow highlight; S9 Fig) differed between ID enzootic and IC epizootic isolates in this lineage (lineage K). This suggests that the evolutionary path to epizootic emergence is likely distinct to each outbreak and virus lineage. To determine whether epizootic sequences from different lineages adopt conserved RNA secondary structure despite the presence of distinct SNPs, consensus RNA structure predictions were generated for each epizootic and enzootic group from lineage M, L, and K using RNAalifold [17,51] (S8 Fig, **D**). While overall the predicted secondary structure differed between all lineages, we observed that the 5' structural element and first conserved structural element (Fig 7B and 7C; highlighted in blue and grey in S10 Fig, **D**) were predicted to be conserved in both IAB and IC epizootic strains. This region encompasses four of the SNPs within the central E1 region responsible for differential macrophage replication, including nt 10,495 which we found was sufficient to increase replication of TC83 to levels similar to TC83/E1$_{ID\text{-}syn}$ (S8 Fig). Collectively, this data shows that SNPs associated with macrophage replication fitness are conserved within lineages. Importantly, RNA structures are predicted to be conserved across epizootic viruses from distinct lineages despite variations in SNPs, suggesting that epizootic VEEV may evolve conserved RNA secondary structures that are functionally relevant for VEEV emergence.

Discussion

Repeated emergence of epidemic/epizootic VEEV as well as the emergence and re-emergence of other viral pathogens in recent times, has highlighted the need to better understand viral and host determinants that drive these processes. For VEEV, widespread vaccination of equines has been significant in the control of epidemic/epizootic outbreaks, though vaccines and therapeutics for use in humans remain a significant gap [52]. Moreover, the ability to produce significant viremia in humans, and the presence of susceptible urban mosquito vectors in VEEV endemic regions suggests significant potential for VEEV to evolve the ability to transmit in urban settings without the need for an equine amplification host. Thus, understanding how host and viral factors drive the evolution and emergence of VEEV and other viral pathogens in nature is paramount. While previous phylogenetic studies have emphasized the importance of amino acid mutations within E2 in the emergence of epizootic VEEV [9,10,53], our data

supports an additional role for RNA structure in viral replication and cellular tropism, which has implications for immune evasion, dissemination, and transmission.

In this study we identified novel RNA structures that alter VEEV replication fitness specifically in macrophages, but not in other cell types. To our knowledge, this is the first time that VEEV RNA structure has been demonstrated to alter cellular tropism. In addition, we identified several RBPs which enhance replication of E1 enzootic mutants, namely THRAP3, UBAP2L, FBL, and DHX38.

To our knowledge, none of these RBPs have previously been shown to play a role in facilitating alphavirus replication, or for the most part, other RNA viruses. While these RBPs have been implicated in a wide variety of cellular functions, they have all been shown play a role in mRNA stability and translation [39–41]. Consistent with these reports, we have demonstrated that changes in E1 sequence and structure increases translation of TC83/$E1_{ID\text{-}syn}$ RNA, which is dependent in part on THRAP3. THRAP3 (thyroid hormone receptor-associated protein 3) is most notably described as an RNA splicing factor [54–57] and has also been implicated in transcriptional regulation [58,59] and RNA stability [60]. However, the mechanisms by which THRAP3 regulate RNA metabolism is poorly described. Interestingly, recent studies have demonstrated a central role for THRAP3 in stress granule assembly [43,44] along with UBAP2L and other notable stress granule-associated proteins (G3BP1/2) [61–65]. While we were unable to conclusively demonstrate a role for UBAP2L in increasing translation of TC83/$E1_{ID\text{-}syn}$ reporter RNA due to significant translational repression following KD in these assays, we clearly observed interaction of this RBP with viral RNA and demonstrated its role in enhanced replication of TC83/$E1_{ID\text{-}syn}$ (**Fig 4G and 4H**). Stress granule assembly dependent on G3BP1/2 and UBAP2L has been suggested to prevent excessive innate immune activation [63], thus in addition to regulation of viral RNA translation, we speculate that recruitment of UBAP2L to the VEEV genome could potentially regulated inflammatory responses, though in a manner that is independent of IFN and ISG expression (**Fig 3**).

At present the precise RNA structures necessary for recruitment of THRAP3 to TC83/$E1_{ID\text{-}syn}$ RNA is unclear and future efforts will focus on defining the precise structural and biochemical determinants of this interaction. Notably, we identified several hairpins in the core region of E1 that are conserved between TC83 and TC83/$E1_{ID\text{-}syn}$ and other strains (**Fig 7B and 7C**, grey boxes; **S10 Fig**) which contain AU-rich and AC-rich loop sequences. Many factors which regulate translation are known to bind to AU-rich and AC-rich sequences [66–70], thus we speculate that conservation of these hairpins may suggest a role for these structures in translation of viral RNA. Whether THRAP3 interacts with these AU/AC-rich elements or functions by altering association of other translation factors with these elements remains to be determined. Defining RNA motifs and the structural basis of THRAP3-RNA recognition during VEEV infection will provide important insight into novel mechanisms of VEEV translational control.

Given the cell type specific nature of the replication phenotype observed, we speculated that the RBPs identified may be expressed preferentially in macrophages compared to other cell types in which TC83 and TC83/$E1_{ID\text{-}syn}$ replicated to similar levels. In contrast to our expectations, we observed that THRAP3, FBL, UBAP2L, and DHX38 were all expressed in both MEF and Raw264.7, but unexpectedly, expression of these RBPs was significantly repressed in MEF, but not macrophages following infection **(S4 Fig, D).** Previous studies have shown that a subpopulation of macrophages is resistant to macromolecular synthesis shutoff following VEEV infection [35]. Given that fibroblasts are sensitive to macromolecular synthesis shutoff, it is logical that these RBPs implicated in translational control (THRAP3, FBL, UBAP2L, and DHX38) would be downregulated in MEF. Thus, while these RBPs are not macrophage-specific per se, they may play a more prominent role in macrophages since these cells are resistant

to translational repression following infection. It is tempting to speculate that VEEV may have evolved to exploit RBPs that regulate translation (such as THRAP3) that are more abundant in macrophages but downregulated in other cell types. Future studies will focus on broadly defining replication phenotypes of epizootic and enzootic VEEV in macrophages and the role of THRAP3 and other RBPs in translation. Whether enhanced replication of other alphaviruses in myeloid cells is also specifically dependent on these RBPs or is more generally regulated by RBPs that control translation remains to be determined.

The observation that macrophage replication is specifically impacted by changes in E1 RNA is highly relevant, as myeloid cells are important targets early during in vivo infection and macrophages are important producers of IFN in this system [24,25]. Notably, we observed that VEEV encoding E1 RNA sequences and RNA structures from an epizootic strain (TC83; IAB) replicated less efficiently in macrophages in relation to enzootic mutants. This is consistent with our prior studies, which similarly demonstrated that VEEV encoding either epizootic or enzootic 3'UTR sequences replicate differentially in an IFIT2-dependent manner [15] and to differences in replication that we have observed between the epizootic derived TC83 and the enzootic strain ZPC738 (**S11 Fig**). While seemingly counterintuitive, we predict that diminished myeloid cell replication is associated with enhanced dissemination and viremia *in vivo*. In our proposed model, enhanced replication of enzootic mutants in myeloid cells in the lymph node leads to enhanced immune activation in neighboring cells which restricts viral replication in the periphery, leading to poor dissemination and viremia, reduced transmission, and possibly reduced pathogenesis. In contrast, epizootic mutants which replicate more poorly in these cells do not induce robust immune responses leading to more efficient dissemination and transmission. This model is also supported by studies with eastern equine encephalitis virus (EEEV), in which increased macrophage replication fitness leads to potent attenuation *in vivo* [24]. While increased macrophage replication with EEEV correlated with enhanced IFN production, we did not observe any significant difference in IFN expression or signaling between WT and E1 mutant VEEV. Nonetheless, we predict that multiple mechanisms (IFN-dependent and -independent) may possibly play a role in VEEV emergence, given the demonstrated role for this cytokine [12,71].

In addition to the 3'UTR and E1, we are also examining how other VEEV RNA sequences and structures may contribute to myeloid cell replication fitness, and how this impacts dissemination, pathogenesis, and transmission. Based on our observations we propose a more complex mechanism of VEEV emergence which entails acquisition of multiple mutations across the genome that collectively facilitate viral entry, replication fitness, and immune evasion in amplification hosts and vector species that facilitate transmission during epizootic episodes. We predict that diminished macrophage replication fitness is a hallmark of epizootic VEEV isolates. Furthermore, we suggest that macrophage replication phenotypes may be a more accurate cell culture-based predictor of epizootic potential, instead of determination by E2 sequences alone. These findings highlight the complexity of factors that contribute to viral emergence and highlight the importance of examining multiple cell types and host factors.

Materials and methods

Cell lines

Vero C1008 and Raw264.7 cells were obtained from ATCC. All cell lines were maintained in DMEM supplemented with 10% heat-inactivated FBS (HyClone), 1% L-GlutaMAX (Gibco), and 1% nonessential amino acids (NEAA).

Bone marrow derived macrophages (BMDMs) and Bone marrow derived dendritic cells (BMDCs) were generated independently from 10 to 20-week-old C57BL/6 mice. The mice

were sacrificed, the femur and tibia were removed and cleaned. The bones were then briefly dipped in 70% EtOH to sterilized, followed by 1x PBS to remove any excess EtOH. The ends of the bones were then cut to expose the bone cavity and the bones were flushed with media using a 26.5G needle. The cells from one mouse were then divided over 3x 10cm non-tissue culture. To generate BMDMs, the dishes were grown in DMEM supplemented with 10% FBS (HyClone), 1% L-GlutaMAX (Gibco), 1% NEAA, 10,000 U/ml penicillin (Sigma), 10 mg/ml streptomycin (Sigma), and 20% L929-conditioned cell supernatant (described below). To generate BMDCs, the dishes were grown in DMEM supplemented 10% FBS (HyClone), 1% L-GlutaMAX (Gibco), 1% NEAA, 10,000 U/ml penicillin (Sigma), 10 mg/ml streptomycin (Sigma), 55mM β-mercaptoethanol and 20ng/ml GM-CSF (). On day 2 post harvesting, BMDMs were supplemented with 7ml BMDM media. On day 3, the cells were harvested by gently washing with PBS, followed by incubation with 10ml of 1mM EDTA in PBS for 5min at 37˚C, and seeded for infection. On day 3 post harvesting, BMDCs were supplemented with 7ml BMDC media. On day 6, the non-adherent cells were harvested and seeded for infection.

The L929-conditioned cell supernatant was prepared by culturing L929 cells in a T175 until 90% confluence. This was then split into 6 new T175 flasks containing 45 ml of supplemented DMEM (10% GBS, 1% NEAA, 1% GluMAX) and cultured for 10 days at 37˚C. Cell supernatants were then collected and centrifuged at 3000 rpm for 3 mins at 4˚C. Lastly, supernatant was filtered using 45μM filter and stored at -20˚C.

Generation of Raw264.7 RIG-I$^{-/-}$ and MDA5$^{-/-}$ CRISPR cells

To make a doxycycline-inducible CRISPR/Cas9 expression vector (pSBtet-puro-Cas9-U6), the Cas9-U6 fragment of pX459 (Addgene #62988; [72] was cloned into pSBtet-pur (Addgene #60507; [73]). Cas9 was first cloned into pSBtet-pur using the following primers: Cas9.F: 5'-CATGAGACCGGTGCCACCATG-3', Cas9.R: 5'-CATGAGGCGGCCGCCTACTTTTT CTTTTTTGCCTGGCCG, pSBtet-pur.F: 5'-CATGAG GCGGCCGCCTTCC-3', pSBtet-pur.R: 5'-CATGAGACCGGTGGTGGCCGATATCTCAGAG. Post cloning, Cas9 was ligated into the pSBtet-pur backbone using the 5' AgeI and 3' NotI restriction sites. Following this, the U6 promoter was cloned into the new plasmid using the following primers: U6.F 5'-ACTACAGG TACC GAGGG-3', U6.R 5'-TCAGTCCTAGGTCTAGAGC-3', pSBtet-pur-Cas9.F 5'-TCAGT CCTAGGTCTAGAGC-3', pSBtet-pur-Cas9.R 5'-ATGAAGGTACCACATTTGTAGAGGT TTTACTTGC-3'. U6 was then ligated into pSBtet-pur-Cas9 using restriction sites 5' KpnI and 3' AvrII. The additional BbsI site in the pSBtet-pur-Cas9 was removed using site directed mutagenesis and the following primers: dBbsI.F 5'-TTGG GAAGAT AATAGCAG-3', dBbsI.R 5'-CTGCTATTATCTTCCCAA-3'.

Sequence-specific gRNA sequences were designed using the Broad Institute Genetic Perturbation Platform gRNA design tool to target mouse Ddx58 and Ifih1. Dhx58 and Ifih1 gRNA oligonucleotides were cloned into pSBtet-puro-Cas9-U6 using the primers in **S1 Table**, as described previously [72].

Raw264.7 CRISPR KO cells were made by electroporating low passage Raw264.7 cells with Dhx58 and Ifih1 pSBtet-puro-Cas9-U6 using Amaxa Nucleofector II and Amaxa Cell Line Nucleofector Kit V (Lonza). Cells were selected with puromycin for 3 days post-nucleofection, and Cas9/gRNA expression was induced at 7 days post-nucleofection. Following this, cells were treated for 14 days with doxycycline and the KO efficiency of the cells was validated by western blotting.

Generation of full-length and recombinant viruses

Construction of the full length TC83 VEEV infectious clone [16] and ZPC738 [74] have been previously described. To introduce the E1 gene from KC344519 into TC83, a gBlock

containing the E1 gene with flanking TC83 regions was generated (S2 Table). The following primers were used to amplify two TC83 backbone fragments from the VEEV TC83 infectious clone described above: TC83 F1: 5'-GCTTGGTGCTGGCTACTATTG-3', TC83 R1: 5'- CTC TTCGGATGCACCCTCAC -3', TC83 F2: 5'- GATGCAGAGCTGGTGAG -3', TC83 R2: 5'- GTTATACGAGATTCCCGCTTGG -3'. The backbone fragments were generated using Q5 high fidelity polymerase (NEB, M0491), followed by overnight treatment with DpnI. The DNA was then purified using MicroElute Cycle-Pure Kit (Omega Bio-Tek). Fragment assembly was performed using Quantabio RepliQa HiFi assembly mix (#95190-D10) followed by transformation into NEB Stable Competent *E. coli*.

Mutants 1–3 were generated as follows. Fragments for mutant 1 were amplified using the following primers with corresponding plasmid: TC83/E1$_{ID\text{-}syn}$ fw 5'-GCAAGATAGACAAC GACG-3' and rv 5' GTCTCTGCAGCACTAGG 3', TC83: fw 5' CTGTATGCCAATACCA ACC 3' and rv 5' CTGGCCCTTTCGTCTTC 3'. Mutant 2 fragments were generated using the same primers, but with the opposite plasmids. Fragments for mutant 3 were generated using the following primers:

TC83/E1$_{ID\text{-}syn}$ fw 5' TTCAATGGGGTCAAAATAACTG 3' and rv 5' GTCAAAGGCTAA TGGAATTGAC 3', TC83 fw 5'GCAAGATAGACAACGACG 3' and rv 5' GGACCTGCAGT TATTTTGAC 3', TC83 fw 5' GTGCTGTAGGGTCAATTCC 3' and rv 5' CTGGCCCTTTCG TCTTC 3'. The fragments were generated and assembled as described above.

Mutants 7–12 were generated using the primers S4 Table. Site-directed mutagenesis was performed using Q5 high fidelity polymerase (NEB, M0491), treated overnight with DpnI and the DNA was purified using Mag-Bind TotalPure NGS beads (Omega Bio-Tek) followed by transformation into NEB Stable Competent *E. coli*.

Plasmids were linearized at MluI restriction sites located downstream of the poly(A) tail and genomic RNA was transcribed from the SP6 promoter in the presence of N7^{m}G cap analog using the SP6 mMessage mMachine kit (Ambion). 1x10^{7} BHK21 cells were electroporated with approximately 2 μg of *in vitro* transcribed RNA using a GenePulser Xcell electroporator (Bio-Rad) to generate P0 virus stocks.

Focus-forming assays

Vero E6 monolayers were infected with serial 10-fold dilutions of infectious samples for 1 hour at 37˚C, then overlaid with 100 μl per well of medium (0.5x DMEM, 5% FBS) containing 1% carboxymethylcellulose, and incubated for 20 to 22 hours at 37˚C with 5% CO_2. Cells were then fixed by adding 100 μl per well of 2% paraformaldehyde directly onto the overlay at RT for 2 hours. After removing the overlay media and fix, cells were washed 3x with 1x PBS and incubated with VEEV E2 glycoprotein specific antibodies (gift of Dr. Michael Diamond) for 2 hours at RT in FFA permeabilization buffer (1x PBS, 0.1% saponin, and 0.1% BSA). Mouse anti-VEEV E2 (clone 36.E5) were generated and purified from a clonal hybridoma cell line, a generous gift from Dr. Michael Diamond (Washington University School of Medicine, St Louis). Cells were washed 3x in ELISA wash buffer (1x PBS, 0.05% triton X-100), then incubated with species-specific HRP-conjugated secondary antibodies (Sigma and ThermoFisher) for 1 hour at RT in FFA permeabilization buffer. Monolayers were washed 3x with ELISA buffer and foci were developed by incubating in 50 μl/well of TrueBlue peroxidase substrate (KPL) for 5 to 10 minutes at RT, after which time cells were washed twice in water. Well were imaged using Immuno Capture software (Cell Technology Ltd.), and foci were subsequently counted using BioSpot software (Cell Technology Ltd.). Samples were titered in duplicate and the average titers were calculated.

Viral growth kinetic assays

Multistep viral growth kinetics were performed by infecting Raw264.7 with WT or mutant VEEV TC83 viruses at a MOI of 0.1. Cells were seeded 18-20hrs prior to infection. Viral titers were determined for indicated time points post-infection by removing cell culture supernatant, replacing it with fresh growth media, and subsequently measuring viral titers through FFA. All experiments were performed three or four times independently in triplicate. Statistical analysis was performed by calculating area under the curve (AUC) and performing unpaired t-test on AUC values calculated for each experiment. P values are reported in each figure.

siRNA knock-down

DsiRNA transfections were done in 96 well format. DsiRNAs used are listed in S3 Table. Transfection mix was made up of 10nM DsiRNA pool, 0.2μl *Trans*IT-X2 Dynamic Delivery System (Mirus, 6003) and supplement-free DMEM and incubated at RT for 20mins. 2E4 Raw264.7 cells were combined with the transfection complexes and seeded into a 96 well plate. 24 hours post transfection were mock infected or infected with either TC83 or TC83/$E1_{ID\text{-}syn}$ at an MOI of 0.1. 24 hours post infection, supernatant was collected and titered as describe previously. Cell viability was then assess using alamarBlue Cell Viability Reagent (Invitrogen, DAL1025) as described by the manufacturer.

IFNAR blocking antibody infections

Raw264.7 cells were seeded 24h prior to infection. One hour prior to infection, the cells were pretreated with 10μg of mouse IgG2a isotype control (InVivoMAb, BE0085) or IFNAR1 Monoclonal Antibody (MAR1-5A3, Invitrogen 16-5945-85), infected with TC83 or TC83/$E1_{ID\text{-}syn}$ at an MOI of 0.1 in the presence of antibody. Infectious virus from cell culture supernatants harvested at 10 and 22 hpi was titered by FFA. Each experiment was performed three times independently. Cell lysates were collected at 22hpi for RT-qPCR analysis.

RT-qPCR

Cell lysates were prepared using Quick-RNA MiniPrep Kit (Zymo Research, Cat# 11–328) according to manufacturer's protocol. Samples were DNase I (NEB, M0303) treated for 20 mins at 37˚C, followed by inactivation of DNase I in 0.1M EDTA for 10 mins at 70˚C. cDNA was generated with 100ng/10μl reaction using iScript cDNA synthesis kit (Bio-rad, 1708890). qPCR was then run with 1μl of cDNA using iTaq Universal Probes Supermix (Bio-rad, 1725130) on Bio-Rad CFX96 Real-Time System. The following primer probe assays were used: Ifit1 (IDT, Mm.PT.58.32674307), IFN-beta (IDT, Mm.PT.58.30132453.g), ISG15 (IDT, Mm.PT.58.41476392.g), VEEVset3 (nt9835-9856) (IDT, probe sequence: /56-FAM/TTT GTC TGG /ZEN/CTG TGC TTT GCT GC/3IABkFQ/), TC83.gRNA (IDT, probe sequence: /56-FAM/AGA AAG CAC /ZEN/AGC GTA AGA GCC GAT /3IABkFQ/) and TC83.sgRNA (IDT, probe sequence: /56-FAM/AGC TGT TAA /ZEN/GTG CCC CGG AAG G/3IABkFQ/).

Western blotting

Cell lysates were generated by washing monolayers with PBS followed by incubation with RIPA lysis buffer (Thermofisher, cat# 89901) supplemented with Halt protease inhibitor cocktail (Thermofisher, cat# 78429) on ice for 5 min. Lysates were then scraped, transferred to microcentrifuge tubes, pulse vortexed and further incubated on ice for 15 mins. Hereafter, lysates were centrifuged at 16,000xg for 20 mins at 4˚C and supernatants were transferred to a

new tube. Proteins were separated by on a 4–20% Mini-PROTEAN TGX precast protein gel (Bio-rad), transferred to a nitrocellulose membrane (Amersham, 10600008), and then labeled for proteins. The following antibodies were used: beta-Actin Mouse mAb (Cell signaling, 8H10D10), beta-Actin Rabbit mAb (Cell signaling, 13E5), Rig-I mAb (Cell signaling, D1466), MDA-5 Rabbit mAb (Cell signaling, D74E4), Fibrillarin/U3 RNP Rabbit pAb (ABclonal, A1136), Dhx38 (ABclonal A4341), Thrap3 Rabbit pAb (ABclonal, A9396), UBAP2L (E5X4E) Rabbit mAb (Cell Signaling Technology, 40199), Goat-anti-Rabbit IRDye 800 (Licor, 926–32211), Goat-anti-mouse IRDye 680 (Licor, 926–68070).

To determine changes in protein expression, the integrated density was measured for each protein of interest band using Adobe Photoshop. Background signal was subtracted. For comparisons between Raw264.7 and iMEF, and when determining the KD efficiency, the integrated density of the protein of interest bands were normalized to the actin loading control and percentage compared to the Raw264.7 uninfected samples or NSC was calculated.

Immunoprecipitation-mass spectrometry

Cell lysates were generated from Raw264.7 cells by resuspending cells in 1X CHAPS lysis buffer (10mM HEPES, 200mM NaCl, 1% CHAPS, 10mM MgCl2, protease inhibitor (Thermo Scientific Pierce, PIA32955), 200U/ml murine RNase inhibitor (NEB, M0314)). Lysates were then passed through a 25G needle 4x and incubated on ice for 15min to ensure lysis. Thereafter, lysates were centrifuged at 16,000xg for 20 mins at 4˚C and supernatants were transferred to a new tube. 50μl of Dynabeads protein G (Thermo, #10003D) were washed 2x in 500μl lysis buffer, after which they were incubated in 200μl lysis buffer along with 12μg of mouse J2 IgG2a Or mouse IgG2a isotype control (InVivoMAb, BE0085) for 30 mins at RT. Beads were then washed 3x in lysis buffer, incubated with 3mg of Raw264.7 lysate on the rotator for 2hrs at RT, washed again 3x in lysis buffer followed by 3x with freshly prepared 20mM ammonium bicarbonate. Samples were then trypsin digested in 20μl 20mM ammonium bicarbonate and incubated with 10μl of 10ng/μl sequencing grade trypsin (Promega, cat# V5111) at 37˚C for 3hrs at 1500rpm. The supernatant was then carefully removed from the beads and the beads where washed 2x in 30μl 20mM ammonium bicarbonate, and all fractions were pooled. Samples were then reduced by adding tris(2-carboxyethyl)phosphine (TCEP) to a final concentration of 1mM and incubated at 37˚C for 1h. Freshly prepared iodoacetamide (Thermo, cat# 90034) was then added to a final concentration of 10mM and incubated at RT for 30min in the dark, followed by quenching with final concentration 2mM N-AcetylCysteine. Samples were then cleaned-up and concentrated using C18 columns (Thermo-Pierce, cat# 89870) according to the manufacturers protocol. After clean-up, formic acid was added to the samples at a final concentration of 0.1%. Samples were analyzed by LC/MS at University of Washington's Proteomics Resource (UWPR).

SHAPE-MaP

VERO cells were seeded at 25E6 cells per 10cm dish. 24 hours post seeding, cells were infected with either TC83 or TC83/E1$_{ID\text{-}syn}$ at MOI 0.1. At 24hpi culture media was aspirated and cells were washed once with 1x PBS. In-cell SHAPE modifications were made by adding fresh 500μl of 100mM 1-Methyl-7-nitroisatoic anhydride (1M7) (Sigma-Aldrich, 908401) in DMSO to 4.5ml pre-warmed culture media to the dish and incubated for 3min at 37C. This was repeated 3x to increase modifications. Unmodified samples were similarly treated with DMSO. After treatment, whole-cell RNA was purified using TRIzol reagent (Fisher Scientific) according to the manufacturers protocol. Samples were treated with TURBO DNase (Thermo Fishter, AM2238) for 30min at 37C to remove any DNA. Polyadenylated RNA was then isolated from

the whole-cell RNA using NEB Oligo d(T)25 Magnetic beads (NEB, S1419S) according to the manufacturers protocol. To generate the denatured controls, 1μg of TC83 DMSO and TC83/$E1_{ID\text{-}syn}$ DMSO polyA purified RNA were heated to 95C for 2min in 1x DC buffer (50mM HEPES (pH 8.0), 4mM EDTA) with an equal volume of 100% formamide. Samples were then immediately transferred to a new tube containing fresh 1M7 to a final concentration of 10mM and heated at 95C for 2min, after which the samples were placed on ice. DC control RNA was then purified using G-50 columns (GE healthcare, 25-5330-01). All samples were then prepared for sequencing using the randomer library prep workflow protocol described in Smola et al. [46]. Samples were sequenced by Illumina NGS at the Fred Hutch Cancer Center genomics core. Sequencing data was analyzed using Shapemapper2 as previously described.

Translation reporter assays

VEEV translation reporters were constructed based on previously described constructs [14, 42]. The E1 gene from TC83 and TC83/$E1_{ID\text{-}syn}$ were cloned into the VRLF reporter plasmid using PacI and NotI (NEB). Plasmids were linearized overnight with NotI. Reporter RNAs were *in vitro* transcribed using HiScribe T7 High Yield RNA Synthesis kit (NEB, E2040) and capped using Vaccinia Capping System (NEB, M2080) according to the manufacturers protocol.

Reporter assays were performed by nucleofecting (Cell Line Nucleofector Kit V, Lonza VCA-1003) 1E6 Raw264.7 with 4μg of either reporter RNA and plated in 12 wells of a 96-well U-bottom plates. Cells were harvested at indicated time points, washed 1x in with PBS and lysed in 1x passive lysis buffer (Promega). Firefly luciferase assays were performed using Luciferase Assay System (Promega) according to the manufacturers protocol. Luciferase activity was measured using a BioTek Synergy luminometer. Experiments were performed 3 times independently in triplicate. The relative light units were normalized to total protein concentration using a BCA Protein assay (Pierce), and further normalized within each experiment to the 30min TC83 sample. Statistical analysis was performed using unpaired t-test. P values are reported in each figure.

For siRNA KD translation reporter assays, 10μl of a 10nM siRNA pool or NSC were mixed in 600μl neat DMEM with 10μl *Trans*IT-X2 Dynamic Delivery System (Mirus, 6003) and incubated at RT for 15mins. Transfection complexes were then added to 4E6 Raw264.7 macrophages in 6ml of growth media in a 10cm dish. Cells were transfected for 24h, after which translation reporter assays were performed as described above.

Replicon assay

To make the VEEV replicon nsp3-nanoluciferase and ORF2-fireflyluciferase reporters, we replaced the GFP in the previously described VEEV/nsp3-GFP reporter virus (a generous gift of Dr. Ilya Frolov) [75]. This was done by PCR amplifying nano-luciferase with primers adding 5' ClaI and 3' NotI restriction sites using Q5 high fidelity polymerase (NEB, M0491): Fw primer: 5' CGACCCACCATCGATTAGGTTCCGGATCAatggtcttcacactcgaag 3', Rv primer: 5' attacgccagaatgcgttcgcTGGGCGGCCGCTGATCCGGAACC3'. VEEV/nsp3-GFP and the PCR amplified nano-luciferase were then digested with ClaI and NotI, and the VEEV/nsp3 backbone (13,341bp) and nano-luciferase fragments were gel purified. The nano-luciferase fragment was then ligated into the VEEV/nsp3 backbone using Instant Sticky-end Ligase Master Mix (NEB, M0370) followed by transformation into NEB Stable Competent *E. coli*. This cloning resulted in TC83/nsp3-nluc. Before introducing Firefly-luciferase into ORF2, the nano-luciferase from pVR21(F)-nluc [24] was first amplified using the following primers: Fw 5' TTGAGGGGCCCCTATAACTCTCTAC 3', Rv 5'

GTCTCGGCCCGGGCATTACGCCAGAATGCGTTCG 3'. This fragment was then introduced into TC83/nsp3-nluc by digesting both the backbone and nano-luciferase fragments with ApaI and SrfI, gel purifying relevant fragments, and ligating using T4 DNA ligase (NEB, M0202) followed by transformation into NEB Stable Competent *E. coli*. This cloning resulted in TC83/nsp3-nluc_ORF2-nluc-SK-E1. To replace the ORF2 nano-luciferase with firefly-luciferase, firefly-luciferase was PCR amplified with primers adding 5'AscI and 3'SrfI restriction sites: Fw 5' gccaaggcgcgccATGGAAGACGCCAAAAACATAAAGAAAGG 3', Rv 5' gccaaggcgcgccATGGAAGACGCCAAAAACATAAAGAAAGG 3'. This fluc fragment was then introduced into TC83/nsp3-nluc_ORF2-nluc-SK-3'UTR by digesting with ApaI and SrfI, gel purifying and ligating using T4 DNA ligase followed by transformation into NEB Stable Competent *E. coli*. This cloning produced the replicon TC83/nsp3-nluc_ORF2-fluc_6K-E1. Lastly, the E1 sequence from TC83/$E1_{ID\text{-}syn}$ was introduced by digesting the TC83/$E1_{ID\text{-}syn}$ plasmid and the new replicon plasmid with SrfI and MluI. The relevant fragments were gel purified and transformed as described above.

Reporter plasmids were linearized overnight with MluI. Reporter RNAs were *in vitro* transcribed using HiScribe T7 High Yield RNA Synthesis kit (NEB, E2040) and capped using Vaccinia Capping System (NEB, M2080) according to the manufacturers protocol.

Reporter assays were performed by nucleofecting (Cell Line Nucleofector Kit V, Lonza VCA-1003) 1E6 Raw264.7 with 4μg of either reporter RNA and divided over 12 wells of a 96-well U-bottom plates. Cells were harvested at indicated time points, washed 1x in with PBS and lysed in 1x passive lysis buffer (Promega). Dual nano and firefly luciferase were measured using Nano-Glo Dual-luciferase reporter assay system (Promega, N1610) according to the manufacturers protocol. Luciferase activity was measured using a BioTek Synergy luminometer. Experiments were performed 3 times independently in triplicate. The relative light units were normalized to total protein concentration using a BCA Protein assay (Pierce). Statistical analysis was performed using unpaired t-test. P values are reported in each figure.

RNA-aptamer affinity purification

RNA constructs encoding the core region of TC83 or TC83/$E1_{ID\text{-}syn}$ from nts 10,516 to 10,808 along with a 3' hepatitis delta virus ribozyme sequence (5'-gctagccatggtcccagcctcctcgctggcggctagtgggcaacatgcttcggcatggcgaatgggac-3) were cloned downstream of the S1m aptamer [76] using BamHI (5') and EcoRI (3') restriction sites. cDNA clones were linearized with either EcoRI (for TC83 and TC83/$E1_{ID\text{-}syn}$ RNAs) or with BamHI (for S1m aptamer only control RNA) and in vitro transcribed using the T7 HiScribe kit (NEB). Transcibed RNA was folded (65˚C for 5 min, cooled at room temperature for 5 min) and bound to MyOne Streptavidin C1 beads (Thermofisher) for 20 min at 4˚C. Beads were washed 4x with CHAPS lysis buffer (10mM HEPES, 200mM NaCl, 1% CHAPS, 10mM MgCl, 1mM DTT, 1x HALT protease and phosphatase inhibitor (Thermofisher), 200 U/mL murine RNase inhibitor (NEB) and precleared Raw264.7 lysates in CHAPS buffer incubated with beads at 4˚C on a rotator for 2 hours. Beads were washed 6x in CHAPS lysis buffer and bound proteins eluted in 4x laemmeli buffer (Bio-rad). $1/5^{th}$ of affinity purified eluate was analyzed by SDS-PAGE and western blot as described above.

All raw data can be found in **S2 Data**.

Supporting information

S1 Table. Primer sequences for generation of RIG-I and MDA5 CRISPR cell lines.
(XLSX)

S2 Table. KC344519 E1 gene block.
(XLSX)

S3 Table. DsiRNA sequences.
(XLSX)

S4 Table. Single point mutant primers.
(XLSX)

S1 Fig. Phylogenetic tree of VEEV IAB, IC and ID subtypes. The optimal phylogenetic tree of lineages K, L and M (previously described in [49]) as determined by the neighborhood-joining method [77]. Shown next to each branch is the percentage of replicate trees in which the associated taxa clustered together in the bootstrap test (1000 replicates).
(TIF)

S2 Fig. Sliding window analysis of the relative structure score (RSS) across the VEEV genome broken up by gene. The RSS was calculated as the minimum free energy (MFE)/ ensemble diversity for each window of 50 nucleotides with a step size of 10. TC83 is shown in red and 307537 is shown in blue. Two standard deviations from the mean was calculated across the entire genome and is represented as a dotted line.
(TIF)

S3 Fig. Validation of CRISPR KO and siRNA KD in Raw 264.7 macrophages. (A) Western blots from Raw264.7 6hrs after treatment +/- 100U/ml msIFN-β. **(B)** Western blot of Raw264-7 after transfection with NSC or protein of interest siRNA siRNA pool (10μM) pool for 24hrs or 48hrs. **(C)** Cell viability was determined using alamarblue Cell Viability Reagent and calculated as a percentage compared to the NSC. **(D)** qPCR was performed for viral RNA and the fold change in viral RNA over TC83 is expressed. Statistical analysis was performed using GraphPad Prism 9, using an unpaired T-test.
(TIF)

S4 Fig. Validation of additional mass spectrometry hits. To evaluate the effect of these genes on viral replication **(A)** Raw264-7 cells were transfected with 10mM of a pool of 3 siRNA targeting proteins of interest for 24hrs, after which they were infected with TC83 or TC83/$E1_{ID\text{-}syn}$. Supernatants were collected at 24hpi and infectious virus was titered using FFA. For visual clarity, the individual siRNAs along with the non-silencing control (NSC) are graphed individually, however the NSC is the same in all graphs. Each experiment was performed in triplicate three times independently and the mean and SD are graphed. **(B)** Western blot of Raw264-7 transfected for 24h or 48h with NSC or protein of interest siRNA pool (10μM). **(C)** Cell viability was determined using alamarblue Cell Viability Reagent and calculated as a percentage compared to the NSC. **(D)** Western blot analysis of Raw264.7 or iMEF +/- TC83 (MOI 0.1) lysates at 24hpi. **(E)** Densitometry was performed using Adobe Photoshop and expression of proteins were normalized to the actin control. The percentage expression was then calculated in relation to the uninfected Raw264.7 control. This is representative of two independent repeats. Statistical analysis was performed using GraphPad Prism 9, using an unpaired T-test. * >0.05, ** >0.001.
(TIF)

S5 Fig. Western blot analysis of NSC and Thrap3 siRNA KD in Raw264.7 macrophage used in translation reporter assay. The integrated density of each of the western blot bands was determined using Adobe Photoshop and normalized to the actin control. The expression

of each protein is displayed as a percentage of the raw264.7 uninfected control.
(TIF)

S6 Fig. Previously described stable RNA structures conserved in SHAPE-MaP informed RNA secondary structure. Previous work by Kutchko *et al.* [47] performed *in vitro* SHAPE--MaP of the enzootic ID VEEV strain, ZPC738, and identified stable RNA structures across the VEEV genome. Displayed here are the SHAPE-MaP informed secondary structure predictions of **(A)** the ribosomal frameshift motif and **(B)** an E1 stem-loop for TC83 and TC83/$E1_{ID\text{-}syn}$. Shaded in grey are the conserved regions identified between the previously described stable structures in ZPC738 and the *in vivo* SHAPE-MaP data generated for TC83 and TC83/$E1_{ID\text{-}syn}$.
(TIF)

S7 Fig. Quality matrixes for SHAPE-MaP for TC83 and TC83/$E1_{IDsyn}$. Mutation rates for modified, untreated and denatured control **(A)** TC83 and D. TC83/$E1_{ID\text{-}syn}$. Read depths for modified, untreated and denatured control **(B)** TC83 and E. TC83/$E1_{ID\text{-}syn}$. The distribution of the SHAPE-MaP reactivities and the standard error of the reads for C. TC83 and F. TC83/$E1_{ID\text{-}syn}$.
(TIF)

S8 Fig. Replication of single point mutants in Raw264.7 macrophages. Mutant viruses were made containing a single point mutation from 307537 in the TC83 backbone. Raw264.7 were infected with single point mutants (MOI 0.1) and supernatants were harvested at 12 **(A)** or 24 **(B)** hpi and infectious virus titered by focus forming assay (FFA). Each experiment was performed in triplicate three times independently and the mean and SD graphed. Statistical analysis was performed using an unpaired T-test.
(TIF)

S9 Fig. Sequence alignment of the core E1 region. Alignment contains VEEV sequences from lineage K, L and M shown in the phylogenetic order determined in S1 Fig. Lineage K sequences are shaded in purple, lineage L sequences are shaded in blue and lineage M sequences are shaded in green. The alignment was made using TC83 (L01443 IAB) as the reference sequence. Varying nucleotides between TC83 and 307537 (KC344519 ID) are highlighted in red in the reference sequence. Identical nucleotides are represented as periods (.).
(EPS)

S10 Fig. TC83 E1 SNPs are conserved in other epizootic strains and are lineage specific. Dot plots from RNAfold [17] predictions of individual SNPs within the E1 core region (10,466–10,843) for **(A)** TC83, **(B)** TC83/$E1_{ID\text{-}syn}$ and **(C)** overlayed dotblots. Yellow boxes highlight regions with differences in RNA structure predictions. **(D)** Predicted RNA secondary structures from RNA alignfold [51]of sequences from lineages K (divided into epizootic IC and enzootic ID), L and M. Steml-loop conserved in epizootic lineages is highlighted in blue, and stem-loop conserved in all lineage K and L highlighted in grey.
(TIF)

S11 Fig. Enzootic ID strain ZPC738 replicates more efficiently than TC83 in macrophages. Replication kinetics of VEEV TC83 and ZPC738 in Raw264.7. Cells were infected with indicated viruses at a MOI of 0.1. Cell culture supernatant was serially harvested at 1, 6, 12, and 24 hpi and infectious virus was titered using focus forming assay (FFA). The experiment was performed in triplicate, three independently and the mean and SD are graphed. Statistical analysis was performed by calculating the area under the curve (AUC) for each replicate, and the AUC

values from TC83 and ZPC738 were analyzed by unpaired t-test.
(TIF)

S12 Fig. RNA aptamer immunoprecipitation of Fbl, Thrap3, Ubap2l and Dhx38. *In vitro* RNAs encoding 4x repeats of the S1m-aptamer followed by the core region of E1 (10,516–10,808) from TC83 or TC83/$E1_{ID\text{-}syn}$ were generated along with a 4x S1m-aptamer only control RNA. RNA was bound to streptavidin beads then incubated with cellular lysates from Raw264.7, and bound proteins eluted and analyzed. **(A)** Western blot analysis of Fbl, Thrap3, Ubap2l and Dhx38 is displayed for the input lysate control, RNA aptamer control, TC83 or TC83/$E1_{ID\text{-}syn}$ aptamer RNAs. **(B)** Densitometry was performed on the bands using Adobe Photoshop and the fold change in density of the TC83/$E1_{ID\text{-}syn}$ over the TC83 RNA aptamer is displayed. This is representative of two independent repeats.
(TIF)

S1 Data. LC-MS screen data. Spectral counts for all targets identified in LC-MS screen (See also Figs 4 and S4).
(XLSX)

S2 Data. Raw data.
(XLSX)

Acknowledgments

The authors thank M.S. Diamond and I. Frolov for their generosity with VEEV reagents.

Author Contributions

Conceptualization: Jennifer L. Hyde.

Formal analysis: Sarah E. Hickson, Jennifer L. Hyde.

Funding acquisition: Jennifer L. Hyde.

Investigation: Sarah E. Hickson, Jennifer L. Hyde.

Methodology: Sarah E. Hickson, Jennifer L. Hyde.

Project administration: Jennifer L. Hyde.

Supervision: Jennifer L. Hyde.

Writing – original draft: Sarah E. Hickson, Jennifer L. Hyde.

Writing – review & editing: Sarah E. Hickson, Jennifer L. Hyde.

References

1. Weaver SC, Ferro C, Barrera R, Boshell J, Navarro JC. Venezuelan equine encephalitis. Annu Rev Entomol. 2004; 49:141–74. Epub 2003/12/04. https://doi.org/10.1146/annurev.ento.49.061802.123422 PMID: 14651460.
2. Ferro C, Boshell J, Moncayo AC, Gonzalez M, Ahumada ML, Kang W, et al. Natural enzootic vectors of Venezuelan equine encephalitis virus, Magdalena Valley, Colombia. Emerg Infect Dis. 2003; 9(1):49–54. Epub 2003/01/21. https://doi.org/10.3201/eid0901.020136 PMID: 12533281; PubMed Central PMCID: PMC2873762.
3. Brault AC, Powers AM, Holmes EC, Woelk CH, Weaver SC. Positively charged amino acid substitutions in the e2 envelope glycoprotein are associated with the emergence of venezuelan equine encephalitis virus. J Virol. 2002; 76(4):1718–30. Epub 2002/01/19. https://doi.org/10.1128/jvi.76.4.1718-1730.2002 PMID: 11799167; PubMed Central PMCID: PMC135911.

4. Brault AC, Powers AM, Weaver SC. Vector infection determinants of Venezuelan equine encephalitis virus reside within the E2 envelope glycoprotein. J Virol. 2002; 76(12):6387–92. Epub 2002/05/22. https://doi.org/10.1128/jvi.76.12.6387-6392.2002 PMID: 12021373; PubMed Central PMCID: PMC136209.
5. Moncayo AC, Lanzaro G, Kang W, Orozco A, Ulloa A, Arredondo-Jimenez J, et al. Vector competence of eastern and western forms of Psorophora columbiae (Diptera: Culicidae) mosquitoes for enzootic and epizootic Venezuelan equine encephalitis virus. Am J Trop Med Hyg. 2008; 78(3):413–21. Epub 2008/03/14. PMID: 18337337.
6. Ronca SE, Dineley KT, Paessler S. Neurological Sequelae Resulting from Encephalitic Alphavirus Infection. Front Microbiol. 2016; 7:959. Epub 2016/07/06. https://doi.org/10.3389/fmicb.2016.00959 PMID: 27379085; PubMed Central PMCID: PMC4913092.
7. Kinney RM, Tsuchiya KR, Sneider JM, Trent DW. Genetic evidence that epizootic Venezuelan equine encephalitis (VEE) viruses may have evolved from enzootic VEE subtype I-D virus. Virology. 1992; 191 (2):569–80. Epub 1992/12/01. https://doi.org/10.1016/0042-6822(92)90232-e PMID: 1448915.
8. Rico-Hesse R, Weaver SC, de Siger J, Medina G, Salas RA. Emergence of a new epidemic/epizootic Venezuelan equine encephalitis virus in South America. Proc Natl Acad Sci U S A. 1995; 92(12):5278–81. Epub 1995/06/06. https://doi.org/10.1073/pnas.92.12.5278 PMID: 7777497; PubMed Central PMCID: PMC41677.
9. Powers AM, Oberste MS, Brault AC, Rico-Hesse R, Schmura SM, Smith JF, et al. Repeated emergence of epidemic/epizootic Venezuelan equine encephalitis from a single genotype of enzootic subtype ID virus. J Virol. 1997; 71(9):6697–705. Epub 1997/09/01. https://doi.org/10.1128/JVI.71.9.6697-6705.1997 PMID: 9261393; PubMed Central PMCID: PMC191949.
10. Greene IP, Paessler S, Austgen L, Anishchenko M, Brault AC, Bowen RA, et al. Envelope glycoprotein mutations mediate equine amplification and virulence of epizootic venezuelan equine encephalitis virus. J Virol. 2005; 79(14):9128–33. Epub 2005/07/05. https://doi.org/10.1128/JVI.79.14.9128-9133.2005 PMID: 15994807; PubMed Central PMCID: PMC1168750.
11. Greene IP, Paessler S, Anishchenko M, Smith DR, Brault AC, Frolov I, et al. Venezuelan equine encephalitis virus in the guinea pig model: evidence for epizootic virulence determinants outside the E2 envelope glycoprotein gene. Am J Trop Med Hyg. 2005; 72(3):330–8. Epub 2005/03/18. PMID: 15772331.
12. Spotts DR, Reich RM, Kalkhan MA, Kinney RM, Roehrig JT. Resistance to alpha/beta interferons correlates with the epizootic and virulence potential of Venezuelan equine encephalitis viruses and is determined by the 5' noncoding region and glycoproteins. J Virol. 1998; 72(12):10286–91. Epub 1998/11/13. https://doi.org/10.1128/JVI.72.12.10286-10291.1998 PMID: 9811777; PubMed Central PMCID: PMC110615.
13. Kinney RM, Johnson BJ, Welch JB, Tsuchiya KR, Trent DW. The full-length nucleotide sequences of the virulent Trinidad donkey strain of Venezuelan equine encephalitis virus and its attenuated vaccine derivative, strain TC-83. Virology. 1989; 170(1):19–30. Epub 1989/05/01. https://doi.org/10.1016/0042-6822(89)90347-4 PMID: 2524126.
14. Hyde JL, Gardner CL, Kimura T, White JP, Liu G, Trobaugh DW, et al. A viral RNA structural element alters host recognition of nonself RNA. Science. 2014; 343(6172):783–7. Epub 2014/02/01. https://doi.org/10.1126/science.1248465 PMID: 24482115; PubMed Central PMCID: PMC4209899.
15. Sarah E. Hickson EB, Schwerk Johannes, Saluhke Indraneel, Zaver Shivam, Woodward Joshua, Savan Ram, Hyde Jennifer L.. Sequence diversity in the 3' untranslated region of alphavirus modulates IFIT2-dependent restriction in a cell type-dependent manner. bioRxiv. 2021. Epub 11 December 2021. https://doi.org/10.1101/2021.12.10.472177.
16. Kinney RM, Chang GJ, Tsuchiya KR, Sneider JM, Roehrig JT, Woodward TM, et al. Attenuation of Venezuelan equine encephalitis virus strain TC-83 is encoded by the 5'-noncoding region and the E2 envelope glycoprotein. J Virol. 1993; 67(3):1269–77. Epub 1993/03/01. https://doi.org/10.1128/JVI.67.3.1269-1277.1993 PMID: 7679745; PubMed Central PMCID: PMC237493.
17. Gruber AR, Lorenz R, Bernhart SH, Neubock R, Hofacker IL. The Vienna RNA websuite. Nucleic Acids Res. 2008; 36(Web Server issue):W70–4. Epub 2008/04/22. https://doi.org/10.1093/nar/gkn188 PMID: 18424795; PubMed Central PMCID: PMC2447809.
18. Zuker M, Stiegler P. Optimal computer folding of large RNA sequences using thermodynamics and auxiliary information. Nucleic Acids Res. 1981; 9(1):133–48. Epub 1981/01/10. https://doi.org/10.1093/nar/9.1.133 PMID: 6163133; PubMed Central PMCID: PMC326673.
19. Wuchty S, Fontana W, Hofacker IL, Schuster P. Complete suboptimal folding of RNA and the stability of secondary structures. Biopolymers. 1999; 49(2):145–65. Epub 1999/03/10. https://doi.org/10.1002/(SICI)1097-0282(199902)49:2<145::AID-BIP4>3.0.CO;2-G PMID: 10070264.

20. McCaskill JS. The equilibrium partition function and base pair binding probabilities for RNA secondary structure. Biopolymers. 1990; 29(6–7):1105–19. Epub 1990/05/01. https://doi.org/10.1002/bip.360290621 PMID: 1695107.

21. Kim DY, Firth AE, Atasheva S, Frolova EI, Frolov I. Conservation of a packaging signal and the viral genome RNA packaging mechanism in alphavirus evolution. J Virol. 2011; 85(16):8022–36. Epub 2011/06/18. https://doi.org/10.1128/JVI.00644-11 PMID: 21680508; PubMed Central PMCID: PMC3147971.

22. Firth AE, Chung BY, Fleeton MN, Atkins JF.Discovery of frameshifting in Alphavirus 6K resolves a 20-year enigma. Virol J. 2008; 5:108. Epub 2008/09/30. https://doi.org/10.1186/1743-422X-5-108 PMID: 18822126; PubMed Central PMCID: PMC2569925.

23. Kendra JA, de la Fuente C, Brahms A, Woodson C, Bell TM, Chen B, et al. Ablation of Programmed -1 Ribosomal Frameshifting in Venezuelan Equine Encephalitis Virus Results in Attenuated Neuropathogenicity. J Virol. 2017; 91(3). Epub 2016/11/18. https://doi.org/10.1128/JVI.01766-16 PMID: 27852852; PubMed Central PMCID: PMC5244343.

24. Gardner CL, Burke CW, Tesfay MZ, Glass PJ, Klimstra WB, Ryman KD. Eastern and Venezuelan equine encephalitis viruses differ in their ability to infect dendritic cells and macrophages: impact of altered cell tropism on pathogenesis. J Virol. 2008; 82(21):10634–46. Epub 2008/09/05. https://doi.org/10.1128/JVI.01323-08 PMID: 18768986; PubMed Central PMCID: PMC2573165.

25. Bhalla N, Sun C, Metthew Lam LK, Gardner CL, Ryman KD, Klimstra WB. Host translation shutoff mediated by non-structural protein 2 is a critical factor in the antiviral state resistance of Venezuelan equine encephalitis virus. Virology. 2016; 496:147–65. Epub 2016/06/19. https://doi.org/10.1016/j.virol.2016.06.005 PMID: 27318152; PubMed Central PMCID: PMC5821108.

26. Frolova EI, Fayzulin RZ, Cook SH, Griffin DE, Rice CM, Frolov I. Roles of nonstructural protein nsP2 and Alpha/Beta interferons in determining the outcome of Sindbis virus infection. J Virol. 2002; 76(22):11254–64. Epub 2002/10/22. https://doi.org/10.1128/jvi.76.22.11254-11264.2002 PMID: 12388685; PubMed Central PMCID: PMC136776.

27. Fragkoudis R, Breakwell L, McKimmie C, Boyd A, Barry G, Kohl A, et al. The type I interferon system protects mice from Semliki Forest virus by preventing widespread virus dissemination in extraneural tissues, but does not mediate the restricted replication of avirulent virus in central nervous system neurons. J Gen Virol. 2007; 88(Pt 12):3373–84. Epub 2007/11/21. https://doi.org/10.1099/vir.0.83191-0 PMID: 18024907.

28. Ryman KD, Meier KC, Gardner CL, Adegboyega PA, Klimstra WB. Non-pathogenic Sindbis virus causes hemorrhagic fever in the absence of alpha/beta and gamma interferons. Virology. 2007; 368(2):273–85. Epub 2007/08/08. https://doi.org/10.1016/j.virol.2007.06.039 PMID: 17681583.

29. Sanchez David RY, Combredet C, Sismeiro O, Dillies MA, Jagla B, Coppee JY, et al. Comparative analysis of viral RNA signatures on different RIG-I-like receptors. Elife. 2016; 5:e11275. Epub 2016/03/25. https://doi.org/10.7554/eLife.11275 PMID: 27011352; PubMed Central PMCID: PMC4841775.

30. Akhrymuk I, Frolov I, Frolova EI. Both RIG-I and MDA5 detect alphavirus replication in concentration-dependent mode. Virology. 2016; 487:230–41. Epub 2015/11/10. https://doi.org/10.1016/j.virol.2015.09.023 PMID: 26550947; PubMed Central PMCID: PMC4721224.

31. Schonborn J, Oberstrass J, Breyel E, Tittgen J, Schumacher J, Lukacs N. Monoclonal antibodies to double-stranded RNA as probes of RNA structure in crude nucleic acid extracts. Nucleic Acids Res. 1991; 19(11):2993–3000. Epub 1991/06/11. https://doi.org/10.1093/nar/19.11.2993 PMID: 2057357; PubMed Central PMCID: PMC328262.

32. Paranjape SM, Harris E. Y box-binding protein-1 binds to the dengue virus 3'-untranslated region and mediates antiviral effects. J Biol Chem. 2007; 282(42):30497–508. Epub 2007/08/30. https://doi.org/10.1074/jbc.M705755200 PMID: 17726010.

33. Varjak M, Saul S, Arike L, Lulla A, Peil L, Merits A. Magnetic fractionation and proteomic dissection of cellular organelles occupied by the late replication complexes of Semliki Forest virus. J Virol. 2013; 87(18):10295–312. Epub 2013/07/19. https://doi.org/10.1128/JVI.01105-13 PMID: 23864636; PubMed Central PMCID: PMC3754020.

34. LaPointe AT, Gebhart NN, Meller ME, Hardy RW, Sokoloski KJ. Identification and Characterization of Sindbis Virus RNA-Host Protein Interactions. J Virol. 2018;92(7). Epub 2018/01/13. https://doi.org/10.1128/JVI.02171-17 PMID: 29321325; PubMed Central PMCID: PMC5972874.

35. Bhalla N, Gardner CL, Downs SN, Dunn M, Sun C, Klimstra WB. Macromolecular Synthesis Shutoff Resistance by Myeloid Cells Is Critical to IRF7-Dependent Systemic Interferon Alpha/Beta Induction after Alphavirus Infection. J Virol. 2019;93(24). Epub 2019/10/04. https://doi.org/10.1128/JVI.00872-19 PMID: 31578290; PubMed Central PMCID: PMC6880179.

36. Garcia-Moreno M, Sanz MA, Carrasco L. A Viral mRNA Motif at the 3'-Untranslated Region that Confers Translatability in a Cell-Specific Manner. Implications for Virus Evolution. Sci Rep. 2016; 6:19217.

Epub 2016/01/13. https://doi.org/10.1038/srep19217 PMID: 26755446; PubMed Central PMCID: PMC4709744.

37. Carrasco L, Sanz MA, Gonzalez-Almela E. The Regulation of Translation in Alphavirus-Infected Cells. Viruses. 2018; 10(2). Epub 2018/02/09. https://doi.org/10.3390/v10020070 PMID: 29419763; PubMed Central PMCID: PMC5850377.

38. Weingarten-Gabbay S, Elias-Kirma S, Nir R, Gritsenko AA, Stern-Ginossar N, Yakhini Z, et al. Comparative genetics. Systematic discovery of cap-independent translation sequences in human and viral genomes. Science. 2016; 351(6270). Epub 2016/01/28. https://doi.org/10.1126/science.aad4939 PMID: 26816383.

39. Decle-Carrasco S, Rodriguez-Pina AL, Rodriguez-Zapata LC, Castano E. Current research on viral proteins that interact with fibrillarin. Mol Biol Rep. 2023; 50(5):4631–43. Epub 2023/03/18. https://doi.org/10.1007/s11033-023-08343-2 PMID: 36928641; PubMed Central PMCID: PMC10018631.

40. Lu JC, Lu CY, Wu YY. THRAP3 depletion reduces PPARgamma mRNA and anti-inflammatory action in 3T3-L1 adipocytes. J Mol Endocrinol. 2021; 67(3):149–59. Epub 2021/08/10. https://doi.org/10.1530/JME-20-0334 PMID: 34370683.

41. Luo EC, Nathanson JL, Tan FE, Schwartz JL, Schmok JC, Shankar A, et al. Large-scale tethered function assays identify factors that regulate mRNA stability and translation. Nat Struct Mol Biol. 2020; 27(10):989–1000. Epub 2020/08/19. https://doi.org/10.1038/s41594-020-0477-6 PMID: 32807991; PubMed Central PMCID: PMC8221285.

42. Tesfay MZ, Yin J, Gardner CL, Khoretonenko MV, Korneeva NL, Rhoads RE, et al. Alpha/beta interferon inhibits cap-dependent translation of viral but not cellular mRNA by a PKR-independent mechanism. J Virol. 2008; 82(6):2620–30. Epub 2007/12/28. https://doi.org/10.1128/JVI.01784-07 PMID: 18160435; PubMed Central PMCID: PMC2259014.

43. Iadevaia V, Burke JM, Eke L, Moller-Levet C, Parker R, Locker N. Novel stress granule-like structures are induced via a paracrine mechanism during viral infection. J Cell Sci. 2022;135(4). Epub 2022/02/01. https://doi.org/10.1242/jcs.259194 PMID: 35098996; PubMed Central PMCID: PMC8976915.

44. Bish R, Cuevas-Polo N, Cheng Z, Hambardzumyan D, Munschauer M, Landthaler M, et al. Comprehensive Protein Interactome Analysis of a Key RNA Helicase: Detection of Novel Stress Granule Proteins. Biomolecules. 2015; 5(3):1441–66. Epub 2015/07/18. https://doi.org/10.3390/biom5031441 PMID: 26184334; PubMed Central PMCID: PMC4598758.

45. Smola MJ, Weeks KM. In-cell RNA structure probing with SHAPE-MaP. Nat Protoc. 2018; 13(6):1181–95. Epub 2018/05/05. https://doi.org/10.1038/nprot.2018.010 PMID: 29725122; PubMed Central PMCID: PMC6402486.

46. Smola MJ, Rice GM, Busan S, Siegfried NA, Weeks KM. Selective 2'-hydroxyl acylation analyzed by primer extension and mutational profiling (SHAPE-MaP) for direct, versatile and accurate RNA structure analysis. Nat Protoc. 2015; 10(11):1643–69. Epub 2015/10/02. https://doi.org/10.1038/nprot.2015.103 PMID: 26426499; PubMed Central PMCID: PMC4900152.

47. Kutchko KM, Madden EA, Morrison C, Plante KS, Sanders W, Vincent HA, et al. Structural divergence creates new functional features in alphavirus genomes. Nucleic Acids Res. 2018; 46(7):3657–70. Epub 2018/01/24. https://doi.org/10.1093/nar/gky012 PMID: 29361131; PubMed Central PMCID: PMC6283419.

48. Medina G, Garzaro DJ, Barrios M, Auguste AJ, Weaver SC, Pujol FH. Genetic diversity of Venezuelan alphaviruses and circulation of a Venezuelan equine encephalitis virus subtype IAB strain during an interepizootic period. Am J Trop Med Hyg. 2015; 93(1):7–10. Epub 2015/05/06. https://doi.org/10.4269/ajtmh.14-0543 PMID: 25940191; PubMed Central PMCID: PMC4497907.

49. Forrester NL, Wertheim JO, Dugan VG, Auguste AJ, Lin D, Adams AP, et al. Evolution and spread of Venezuelan equine encephalitis complex alphavirus in the Americas. PLoS Negl Trop Dis. 2017; 11(8):e0005693. Epub 2017/08/05. https://doi.org/10.1371/journal.pntd.0005693 PMID: 28771475; PubMed Central PMCID: PMC5557581 following competing interests: David Lin, Kumar Hari and Ravi Jain work for cBio.

50. Gardner SN, McLoughlin K, Be NA, Allen J, Weaver SC, Forrester N, et al. Characterization of Genetic Variability of Venezuelan Equine Encephalitis Viruses. PLoS One. 2016; 11(4):e0152604. Epub 2016/04/08. https://doi.org/10.1371/journal.pone.0152604 PMID: 27054586; PubMed Central PMCID: PMC4824352.

51. Bernhart SH, Hofacker IL, Will S, Gruber AR, Stadler PF. RNAalifold: improved consensus structure prediction for RNA alignments. BMC Bioinformatics. 2008; 9:474. Epub 2008/11/19. https://doi.org/10.1186/1471-2105-9-474 PMID: 19014431; PubMed Central PMCID: PMC2621365.

52. Powers AM, Williamson LE, Carnahan RH, Crowe JE, Jr., Hyde JL, Jonsson CB, et al. Developing a Prototype Pathogen Plan and Research Priorities for the Alphaviruses. J Infect Dis. 2023; 228(Suppl 6):S414–S26. Epub 2023/10/18. https://doi.org/10.1093/infdis/jiac326 PMID: 37849399.

53. Wang E, Barrera R, Boshell J, Ferro C, Freier JE, Navarro JC, et al. Genetic and phenotypic changes accompanying the emergence of epizootic subtype IC Venezuelan equine encephalitis viruses from an enzootic subtype ID progenitor. J Virol. 1999; 73(5):4266–71. Epub 1999/04/10. https://doi.org/10.1128/JVI.73.5.4266-4271.1999 PMID: 10196323; PubMed Central PMCID: PMC104206.

54. Vohhodina J, Barros EM, Savage AL, Liberante FG, Manti L, Bankhead P, et al. The RNA processing factors THRAP3 and BCLAF1 promote the DNA damage response through selective mRNA splicing and nuclear export. Nucleic Acids Res. 2017; 45(22):12816–33. Epub 2017/11/08. https://doi.org/10.1093/nar/gkx1046 PMID: 29112714; PubMed Central PMCID: PMC5728405.

55. Marcheva B, Perelis M, Weidemann BJ, Taguchi A, Lin H, Omura C, et al. Erratum: A role for alternative splicing in circadian control of exocytosis and glucose homeostasis. Genes Dev. 2021; 35(5–6):425. Epub 2021/03/03. https://doi.org/10.1101/gad.348303.121 PMID: 33649163; PubMed Central PMCID: PMC7919415.

56. Varia S, Potabathula D, Deng Z, Bubulya A, Bubulya PA. Btf and TRAP150 have distinct roles in regulating subcellular mRNA distribution. Nucleus. 2013; 4(3):229–40. Epub 2013/06/20. https://doi.org/10.4161/nucl.25187 PMID: 23778535; PubMed Central PMCID: PMC3720753.

57. Jonsson J, Wang L, Kajitani N, Schwartz S. A novel HPV16 splicing enhancer critical for viral oncogene expression and cell immortalization. Nucleic Acids Res. 2024; 52(1):316–36. Epub 2023/11/23. https://doi.org/10.1093/nar/gkad1099 PMID: 37994701; PubMed Central PMCID: PMC10783526.

58. Choi JH, Choi SS, Kim ES, Jedrychowski MP, Yang YR, Jang HJ, et al. Thrap3 docks on phosphoserine 273 of PPARgamma and controls diabetic gene programming. Genes Dev. 2014; 28(21):2361–9. Epub 2014/10/16. https://doi.org/10.1101/gad.249367.114 PMID: 25316675; PubMed Central PMCID: PMC4215181.

59. Ino Y, Arakawa N, Ishiguro H, Uemura H, Kubota Y, Hirano H, et al. Phosphoproteome analysis demonstrates the potential role of THRAP3 phosphorylation in androgen-independent prostate cancer cell growth. Proteomics. 2016; 16(7):1069–78. Epub 2016/02/04. https://doi.org/10.1002/pmic.201500365 PMID: 26841317.

60. Bracken CP, Wall SJ, Barre B, Panov KI, Ajuh PM, Perkins ND. Regulation of cyclin D1 RNA stability by SNIP1. Cancer Res. 2008; 68(18):7621–8. Epub 2008/09/17. https://doi.org/10.1158/0008-5472.CAN-08-1217 PMID: 18794151; PubMed Central PMCID: PMC2546513.

61. Riggs CL, Kedersha N, Amarsanaa M, Zubair SN, Ivanov P, Anderson P. UBAP2L contributes to formation of P-bodies and modulates their association with stress granules. J Cell Biol. 2024; 223(10). Epub 2024/07/15. https://doi.org/10.1083/jcb.202307146 PMID: 39007803; PubMed Central PMCID: PMC11248227 submitted work. No other disclosures were reported.

62. Cirillo L, Cieren A, Barbieri S, Khong A, Schwager F, Parker R, et al. UBAP2L Forms Distinct Cores that Act in Nucleating Stress Granules Upstream of G3BP1. Curr Biol. 2020; 30(4):698–707 e6. Epub 2020/01/21. https://doi.org/10.1016/j.cub.2019.12.020 PMID: 31956030.

63. Paget M, Cadena C, Ahmad S, Wang HT, Jordan TX, Kim E, et al. Stress granules are shock absorbers that prevent excessive innate immune responses to dsRNA. Mol Cell. 2023; 83(7):1180–96 e8. Epub 2023/04/08. https://doi.org/10.1016/j.molcel.2023.03.010 PMID: 37028415; PubMed Central PMCID: PMC10170497.

64. An H, Tan JT, Shelkovnikova TA. Stress granules regulate stress-induced paraspeckle assembly. J Cell Biol. 2019; 218(12):4127–40. Epub 2019/10/23. https://doi.org/10.1083/jcb.201904098 PMID: 31636118; PubMed Central PMCID: PMC6891081.

65. Youn JY, Dunham WH, Hong SJ, Knight JDR, Bashkurov M, Chen GI, et al. High-Density Proximity Mapping Reveals the Subcellular Organization of mRNA-Associated Granules and Bodies. Mol Cell. 2018; 69(3):517–32 e11. Epub 2018/02/06. https://doi.org/10.1016/j.molcel.2017.12.020 PMID: 29395067.

66. Otsuka H, Fukao A, Funakami Y, Duncan KE, Fujiwara T. Emerging Evidence of Translational Control by AU-Rich Element-Binding Proteins. Front Genet. 2019; 10:332. Epub 2019/05/24. https://doi.org/10.3389/fgene.2019.00332 PMID: 31118942; PubMed Central PMCID: PMC6507484.

67. Hake LE, Mendez R, Richter JD. Specificity of RNA binding by CPEB: requirement for RNA recognition motifs and a novel zinc finger. Mol Cell Biol. 1998; 18(2):685–93. Epub 1998/02/03. https://doi.org/10.1128/MCB.18.2.685 PMID: 9447964; PubMed Central PMCID: PMC108779.

68. Cruz-Gallardo I, Aroca A, Gunzburg MJ, Sivakumaran A, Yoon JH, Angulo J, et al. The binding of TIA-1 to RNA C-rich sequences is driven by its C-terminal RRM domain. RNA Biol. 2014; 11(6):766–76. Epub 2014/05/16. https://doi.org/10.4161/rna.28801 PMID: 24824036; PubMed Central PMCID: PMC4156507.

69. Sokoloski KJ, Dickson AM, Chaskey EL, Garneau NL, Wilusz CJ, Wilusz J. Sindbis virus usurps the cellular HuR protein to stabilize its transcripts and promote productive infections in mammalian and

mosquito cells. Cell Host Microbe. 2010; 8(2):196–207. Epub 2010/08/17. https://doi.org/10.1016/j.chom.2010.07.003 PMID: 20709296; PubMed Central PMCID: PMC2929003.

70. Stickeler E, Fraser SD, Honig A, Chen AL, Berget SM, Cooper TA. The RNA binding protein YB-1 binds A/C-rich exon enhancers and stimulates splicing of the CD44 alternative exon v4. EMBO J. 2001; 20 (14):3821–30. Epub 2001/07/12. https://doi.org/10.1093/emboj/20.14.3821 PMID: 11447123; PubMed Central PMCID: PMC125550.

71. Jahrling PB, Navarro E, Scherer WF. Interferon induction and sensitivity as correlates to virulence of Venezuelan encephalitis viruses for hamsters. Arch Virol. 1976; 51(1–2):23–35. Epub 1976/01/01. https://doi.org/10.1007/BF01317831 PMID: 962587

72. Ran FA, Hsu PD, Wright J, Agarwala V, Scott DA, Zhang F. Genome engineering using the CRISPR-Cas9 system. Nat Protoc. 2013; 8(11):2281–308. Epub 2013/10/26. https://doi.org/10.1038/nprot.2013.143 PMID: 24157548; PubMed Central PMCID: PMC3969860.

73. Kowarz E, Loscher D, Marschalek R. Optimized Sleeping Beauty transposons rapidly generate stable transgenic cell lines. Biotechnol J. 2015; 10(4):647–53. Epub 2015/02/05. https://doi.org/10.1002/biot.201400821 PMID: 25650551.

74. Anishchenko M, Paessler S, Greene IP, Aguilar PV, Carrara AS, Weaver SC. Generation and characterization of closely related epizootic and enzootic infectious cDNA clones for studying interferon sensitivity and emergence mechanisms of Venezuelan equine encephalitis virus. J Virol. 2004; 78(1):1–8. Epub 2003/12/13. https://doi.org/10.1128/jvi.78.1.1-8.2004 PMID: 14671082; PubMed Central PMCID: PMC303380.

75. Foy NJ, Akhrymuk M, Shustov AV, Frolova EI, Frolov I. Hypervariable domain of nonstructural protein nsP3 of Venezuelan equine encephalitis virus determines cell-specific mode of virus replication. J Virol. 2013; 87(13):7569–84. Epub 2013/05/03. https://doi.org/10.1128/JVI.00720-13 PMID: 23637407; PubMed Central PMCID: PMC3700263.

76. Leppek K, Stoecklin G. An optimized streptavidin-binding RNA aptamer for purification of ribonucleoprotein complexes identifies novel ARE-binding proteins. Nucleic Acids Res. 2014; 42(2):e13. Epub 2013/10/26. https://doi.org/10.1093/nar/gkt956 PMID: 24157833; PubMed Central PMCID: PMC3902943.

77. Saitou N, Nei M. The neighbor-joining method: a new method for reconstructing phylogenetic trees. Mol Biol Evol. 1987; 4(4):406–25. Epub 1987/07/01. https://doi.org/10.1093/oxfordjournals.molbev.a040454 PMID: 3447015.